Spectral Analysis of Finite Difference Meshes

Stefan Bilbao

December 28, 2005

Contents

1 Introduction

In this appendix from [2], we reexamine the finite difference schemes corresponding to waveguide meshes discussed in Chapter 4 of [2] in the special case for which the underlying model problem is lossless, source-free, and does not exhibit any material parameter variation. In this case, these finite difference schemes will solve the wave equation, given by

$$\frac{\partial^2 u}{\partial t^2} = \gamma^2 \nabla^2 u \tag{1}$$

in either (2+1)D or (3+1)D, depending on the type of mesh. Here, γ is the *wave speed*, and ∇^2 is the *Laplacian* [6]. These schemes will be linear and shift-invariant, and as such, it is possible to analyze them in the frequency domain, through what is called *Von Neumann analysis* [8]. We will apply these methods to the rectilinear, interpolated rectilinear, triangular, hexagonal and fourth-order accurate schemes in (2+1)D, then to the cubic rectilinear, interpolated cubic rectilinear, octahedral and tetrahedral schemes in (3+1)D.

2 Von Neumann Analysis of Difference Schemes

In this section, we summarize the basics of Von Neumann analysis provided in [8]. Consider the (N+1)D real-valued grid function $U_{\mathbf{m}}(n)$, defined for integer n and for $\mathbf{m} = [m_1, \ldots, m_N] \in \mathbb{Z}^N$, the set of all integer N-tuples. Such a grid function will be used, in a finite difference scheme, as an approximation to the continuous solution $u(\mathbf{x}, t)$ to some problem, at the location $\mathbf{x} = \mathbf{m}\Delta$, and at time $t = nT$, where Δ is the grid spacing, and T is the time step. Here, and henceforth in this appendix, we have assumed that the grid spacing is uniform in all the spatial coordinates, and that the spatial domain is unbounded. We define the space step/time step ratio to be

$$v_0 \triangleq \frac{\Delta}{T}$$

The spatial Fourier transform of $U_{\mathbf{m}}(n)$ is defined by

$$\hat{U}_{\boldsymbol{\beta}}(n) = \frac{1}{(2\pi)^{N/2}} \sum_{\mathbf{m} \in \mathbb{Z}^N} e^{-i\Delta \mathbf{m} \cdot \boldsymbol{\beta}} U_{\mathbf{m}}(n) \Delta^N$$

and is a periodic function of $\boldsymbol{\beta} = [\beta_1, \ldots, \beta_N]^T$, a vector of spatial wavenumbers. The transform can be inverted by

$$U_{\mathbf{m}}(n) = \frac{1}{(2\pi)^{N/2}} \int_{[-\pi/\Delta, \pi/\Delta]^N} e^{i\Delta \mathbf{m} \cdot \boldsymbol{\beta}} \hat{U}_{\boldsymbol{\beta}}(n) d\beta_1 d\beta_2 \ldots d\beta_N$$

where $\boldsymbol{\beta} \in [-\pi/\Delta, \pi/\Delta]^N$ refers to the space enclosed by the intervals $-\pi/\Delta \leq \beta_j \leq \pi/\Delta$, for $j = 1, \ldots, N$. If, for a given grid spacing Δ, we define the discrete spatial L_2 norm of $U_{\mathbf{m}}(n)$ by

$$\|U(n)\|_2 = \left(\sum_{\mathbf{m} \in \mathbb{Z}^N} U_{\mathbf{m}}^2(n) \Delta^N \right)^{1/2}$$

and the corresponding spectral L_2 norm of $\hat{U}_{\boldsymbol{\beta}}(n)$ by

$$\|\hat{U}(n)\|_2 = \left(\int_{[-\pi/\Delta, \pi/\Delta]^N} |\hat{U}_{\boldsymbol{\beta}}(n)|^2 d\beta_1 d\beta_2 \dots d\beta_N \right)^{1/2}$$

then if $U_{\mathbf{m}}(n)$ and $\hat{U}_{\boldsymbol{\beta}}(n)$ are in their respective L_2 spaces, *Parseval's relation* gives

$$\|U(n)\|_2 = \|\hat{U}(n)\|_2$$

2.1 One-step Schemes

Consider the following *one-step* explicit difference scheme, which relates values of the grid function $U_{\mathbf{m}}(n+1)$ to values at the previous time step:

$$U_{\mathbf{m}}(n+1) = \sum_{\mathbf{k} \in \mathbb{K}} \alpha_{\mathbf{k}} U_{\mathbf{m}-\mathbf{k}}(n)$$

where $\mathbb{K}$ is some subset of $\mathbb{Z}^N$, and the parameters $\alpha_{\mathbf{k}}$ are constants; it is initialized by setting $U_{\mathbf{m}}(0)$ equal to some function $U_{\mathbf{m},0}$ (assumed to be in L_2). Taking the spatial Fourier transform of this recursion gives

$$\begin{aligned} \hat{U}_{\boldsymbol{\beta}}(n+1) &= \left(\sum_{\mathbf{k} \in \mathbb{K}} \alpha_{\mathbf{k}} e^{-j\Delta \mathbf{k} \cdot \boldsymbol{\beta}} \right) \hat{U}_{\boldsymbol{\beta}}(n) \\ &= G_{\boldsymbol{\beta}} \quad \hat{U}_{\boldsymbol{\beta}}(n) \end{aligned} \tag{2}$$

$G_{\boldsymbol{\beta}}$ so defined is called the *spectral amplification factor* for a one-step finite difference scheme. (2) implies that we have, in particular, that

$$\hat{U}_{\boldsymbol{\beta}}(n+1) = G_{\boldsymbol{\beta}}^{n+1} \hat{U}_{\boldsymbol{\beta},0} \tag{3}$$

where $\hat{U}_{\boldsymbol{\beta},0}$ is the spatial Fourier transform of the initial condition $U_{\mathbf{m},0}$. (3) further implies that

$$\|\hat{U}(n+1)\|_2 \leq \left(\max_{\boldsymbol{\beta}} |G_{\boldsymbol{\beta}}| \right)^{n+1} \|\hat{U}_0\|_2$$

and finally, through Parseval's relation, that

$$\|U(n+1)\|_2 \leq \left(\max_{\boldsymbol{\beta}} |G_{\boldsymbol{\beta}}| \right)^{n+1} \|U_0\|_2$$

If the $\alpha_{\mathbf{k}}$ which define the difference scheme are independent of the grid spacing and the time step, then such a difference scheme is called *stable* if

$$\max_{\boldsymbol{\beta}} |G_{\boldsymbol{\beta}}| \leq 1$$

The L_2 norm of the solution to the difference equation will thus not increase as the simulation progresses.

2.2 Multi-step Schemes

Multi-step methods can be treated in a very similar way. An explicit M-step method is defined by

$$U_{\mathbf{m}}(n+1) = \sum_{r=1}^{M} \sum_{\mathbf{k} \in \mathbb{K}_r} \alpha_{\mathbf{k}} U_{\mathbf{m}-\mathbf{k}}(n+1-r)$$

for constant coefficients $\alpha_{\mathbf{k}}$ contained in subsets $\mathbb{K}_r$ of $\mathbb{Z}^N$. Taking the Fourier transform of this recursion gives

$$\hat{U}_{\boldsymbol{\beta}}(n+1) = \sum_{r=1}^{M} \sum_{\mathbf{k} \in \mathbb{K}_r} \alpha_{\mathbf{k}} e^{-i\Delta\mathbf{k}\cdot\boldsymbol{\beta}} \hat{U}_{\boldsymbol{\beta}}(n+1-r) \tag{4}$$

A simple way of examining (4) is to look for solutions of the form $\hat{U}_{\boldsymbol{\beta}}(q) = G_{\boldsymbol{\beta}}^q \hat{U}_{\boldsymbol{\beta}}(0)$. This gives the *amplification polynomial equation*

$$G_{\boldsymbol{\beta}}^M = \sum_{r=1}^{M} \sum_{\mathbf{k} \in \mathbb{K}_r} \alpha_{\mathbf{k}} e^{-i\Delta\mathbf{k}\cdot\boldsymbol{\beta}} G_{\boldsymbol{\beta}}^{M-r}$$

the solutions of which, $G_{\boldsymbol{\beta},\nu}$, $\nu = 1, \ldots, M$ must be bounded by unity for stability (though in general, this is not sufficient, as we will show presently for a special case).

A particular form of the amplification polynomial equation which will appear frequently in our subsequent treatment of finite difference schemes for the wave equation is that of a simple two-step centered difference approximation, namely

$$G_{\boldsymbol{\beta}}^2 + B_{\boldsymbol{\beta}} G_{\boldsymbol{\beta}} + 1 = 0 \tag{5}$$

for some real function $B_{\boldsymbol{\beta}}$. This expression has solutions

$$G_{\boldsymbol{\beta},\pm} = \frac{1}{2}\left(-B_{\boldsymbol{\beta}} \pm \sqrt{B_{\boldsymbol{\beta}}^2 - 4}\right) \tag{6}$$

which will be bounded by (and in fact equal to) unity in magnitude if we have $|B_{\boldsymbol{\beta}}| \leq 2$ for all $\boldsymbol{\beta}$. Furthermore, if $|B_{\boldsymbol{\beta}}| > 2$ for some $\boldsymbol{\beta}$, then we will necessarily have an amplification factor with magnitude greater than one at that frequency. For any $\boldsymbol{\beta}$ for which $G_{\boldsymbol{\beta},\pm}$ are not equal, we can write

$$\hat{U}_{\boldsymbol{\beta}}(n+1) = \frac{G_{\boldsymbol{\beta},-}\hat{U}_{\boldsymbol{\beta},0} - \hat{U}_{\boldsymbol{\beta},1}}{G_{\boldsymbol{\beta},-} - G_{\boldsymbol{\beta},+}} G_{\boldsymbol{\beta},+}^{n+1} + \frac{G_{\boldsymbol{\beta},+}\hat{U}_{\boldsymbol{\beta},0} - \hat{U}_{\boldsymbol{\beta},1}}{G_{\boldsymbol{\beta},+} - G_{\boldsymbol{\beta},-}} G_{\boldsymbol{\beta},-}^{n+1}$$

where $\hat{U}_{\boldsymbol{\beta},0}$ and $\hat{U}_{\boldsymbol{\beta},1}$ are the spatial frequency spectra of the two grid functions (at time steps $n = 0$ and $n = 1$) used to initialize the two-step method. It is easy to show that the L_2 norm of $U_{\mathbf{m}}(n)$ can be bounded in terms of the norms of the initial conditions if the spectral amplification factors are distinct and bounded by 1 in magnitude at all wavenumbers.

It is important to realize, however, that the condition that these roots $G_{\boldsymbol{\beta},\pm}$ be bounded by unity is necessary, but not sufficient to ensure no growth in the L_2 norm of the solution; this point has not been addressed in the finite difference treatment of waveguide meshes. In fact, as shown in [2], the simple centered difference approximation to the wave equation admits linearly growing solutions.

This behavior can be examined in the spectral domain as we will now show, as per [8]. Notice that the solutions (6) of the amplification polynomial equation for the two-step scheme can coincide if, and only if at some frequency $\boldsymbol{\beta} = \boldsymbol{\beta}_0$, $B_{\boldsymbol{\beta_0}} = \pm 2$, in which case we have $G_{\boldsymbol{\beta_0},+} = G_{\boldsymbol{\beta_0},-} = \mp 1$. The evolution of the particular spatial frequency component at frequency $\boldsymbol{\beta}_0$ can be written as

$$\hat{U}_{\boldsymbol{\beta_0}}(n) = (\mp 1)^n \hat{U}_{\boldsymbol{\beta_0},0} + n(\mp 1)^{n-1} \left(\hat{U}_{\boldsymbol{\beta_0},1} \pm \hat{U}_{\boldsymbol{\beta_0},0} \right)$$

We can thus expect some linear growth at any such frequency $\boldsymbol{\beta}_0$ if we do not properly initialize the algorithm, so as to cancel the linearly growing part of the solution. It also follows that in employing such a method, one may need to be particularly careful when applying an excitation which contains such frequency components, and that nonlinear signal quantization may pump energy into such modes, even if none is originally present there.

Strikwerda does not classify such linear growth as unstable, because the wave equation itself admits, in addition to traveling wave solutions, a solution which grows linearly with time[2]. For the physical modelling of musical instruments and acoustic spaces, however (the problems to which finite difference schemes of the form to be discussed shortly are usually applied), such solutions are nonphysical and definitely not acceptable. These comments concerning this mild linear instability apply to schemes in unbounded domains; when boundary conditions are present, further analysis will be required.

In order to simplify the analysis of these schemes, we mention that for difference schemes for the wave equation, it is often possible to write

$$B_{\boldsymbol{\beta}} = -2\lambda^2 F_{\boldsymbol{\beta}} - 2 \tag{7}$$

where $\lambda^2 \triangleq \gamma^2 / v_0^2$ and $F_{\boldsymbol{\beta}}$ is independent of λ. In this case, the stability condition can be rewritten as

$$\max_{\boldsymbol{\beta}} |B_{\boldsymbol{\beta}}| \leq 2 \qquad \Longleftrightarrow \qquad \max_{\boldsymbol{\beta}} |\lambda^2 F_{\boldsymbol{\beta}} + 1| \leq 1$$

This new condition on $F_{\boldsymbol{\beta}}$ is easier to analyze: we first require

$$\max_{\boldsymbol{\beta}} F_{\boldsymbol{\beta}} \leq 0 \tag{8}$$

and if (8) holds, we get a further bound on λ, namely

$$\lambda \leq \sqrt{\frac{-2}{\min_{\boldsymbol{\beta}} F_{\boldsymbol{\beta}}}} \qquad \Longrightarrow \qquad T \leq \frac{\Delta}{\gamma} \sqrt{\frac{-2}{\min_{\boldsymbol{\beta}} F_{\boldsymbol{\beta}}}} \tag{9}$$

Thus the stability of these schemes can be simply analyzed in terms of the global maximum and minimum of $F_{\boldsymbol{\beta}}$.

For certain schemes (in particular, the interpolated schemes to be discussed in §3.2 and §4.3), the function $F_{\boldsymbol{\beta}}$ depends on several parameters. Condition (8) tells us the the range of parameters over which our scheme is stable, and over the stability region, condition (9) gives us a maximum time step T, in terms of the grid spacing Δ.

[2] $u = t$, for instance, satisfies (1).

2.3 Vector Schemes

For two of the schemes that we will examine (hexagonal and tetrahedral), it will be necessary to analyze a vectorized system of difference equations. In general, the analysis of vector forms is considerably more difficult; the typical approach will invoke the *Kreiss Matrix Theorem* [8], which is a set of equivalent conditions which can be used to check the boundedness of a particular amplification matrix. In the general vector case we will be analyzing the evolution of a q-element vector $\hat{\mathbf{U}}_{\boldsymbol{\beta}}(n) = [\hat{U}_{1,\boldsymbol{\beta}}(n), \ldots, \hat{U}_{q,\boldsymbol{\beta}}(n)]^T$ of spatially Fourier-transformed functions of $\boldsymbol{\beta}$. The L_2 norm is defined by

$$\|\hat{\mathbf{U}}(n)\|_2 = \left(\int_{[\pi/\Delta, \pi/\Delta]^N} \hat{\mathbf{U}}^*_{\boldsymbol{\beta}}(n) \hat{\mathbf{U}}_{\boldsymbol{\beta}}(n) d\beta_1 d\beta_2 \ldots d\beta_N \right)^{1/2}$$

where * denotes transpose conjugation.

The schemes for the wave equation that we will examine, however, have a relatively simple form. The column vector of grid spatial frequency spectra $\hat{\mathbf{U}}_{\boldsymbol{\beta}}(n)$ satisfies an equation of the form

$$\hat{\mathbf{U}}_{\boldsymbol{\beta}}(n+1) + \mathbf{B}_{\boldsymbol{\beta}} \hat{\mathbf{U}}_{\boldsymbol{\beta}}(n) + \hat{\mathbf{U}}_{\boldsymbol{\beta}}(n-1) = \mathbf{0} \tag{10}$$

for some Hermitian matrix function of $\boldsymbol{\beta}$, $\mathbf{B}_{\boldsymbol{\beta}}$. Because $\mathbf{B}_{\boldsymbol{\beta}}$ is Hermitian, we may write $\mathbf{B}_{\boldsymbol{\beta}} = \mathbf{J}^*_{\boldsymbol{\beta}} \boldsymbol{\Lambda}_{\boldsymbol{\beta}} \mathbf{J}_{\boldsymbol{\beta}}$, for some unitary matrix $\mathbf{J}_{\boldsymbol{\beta}}$, and a real diagonal matrix $\boldsymbol{\Lambda}_{\boldsymbol{\beta}}$ containing the eigenvalues of $\mathbf{B}_{\boldsymbol{\beta}}$. As such, we may change variables via $\hat{\mathbf{V}}_{\boldsymbol{\beta}}(n) = \mathbf{J}_{\boldsymbol{\beta}} \hat{\mathbf{U}}_{\boldsymbol{\beta}}(n)$, to get

$$\hat{\mathbf{V}}_{\boldsymbol{\beta}}(n+1) + \boldsymbol{\Lambda}_{\boldsymbol{\beta}} \hat{\mathbf{V}}_{\boldsymbol{\beta}}(n) + \hat{\mathbf{V}}_{\boldsymbol{\beta}}(n-1) = \mathbf{0} \tag{11}$$

The system thus decouples into a system of scalar two-step spectral update equations; because $\hat{\mathbf{U}}_{\boldsymbol{\beta}}(n)$ and $\hat{\mathbf{V}}_{\boldsymbol{\beta}}(n)$ are related by a unitary transformation, we have $\|\hat{\mathbf{U}}(n)\|_2 = \|\hat{\mathbf{V}}(n)\|_2$, and we may apply stability tests to the uncoupled system (11). We thus require that the eigenvalues of $\mathbf{B}_{\boldsymbol{\beta}}$, namely $\Lambda_{\boldsymbol{\beta},j}$ for $j = 1, \ldots, q$, which are the elements on the diagonal of $\boldsymbol{\Lambda}_{\boldsymbol{\beta}}$, all satisfy

$$\max_{\boldsymbol{\beta}} |\Lambda_{\boldsymbol{\beta},j}| \leq 2 \tag{12}$$

At frequencies $\boldsymbol{\beta}_0$ for which any of the eigenvalues satisfies (12) with equality, then we may again have the same problem with mild linear growth in the solution.

2.4 Numerical Phase Velocity

For a given amplification factor $G_{\boldsymbol{\beta}}$, the *numerical phase velocity* at frequency $\boldsymbol{\beta}$ is defined by

$$v_{\boldsymbol{\beta},phase} = \left| \frac{\log(G_{\boldsymbol{\beta}}/|G_{\boldsymbol{\beta}}|)}{i\|\boldsymbol{\beta}\|_2 T} \right|$$

where $\|\boldsymbol{\beta}\|_2$ is the Euclidean norm of the vector $\boldsymbol{\beta}$. This expression gives the speed of propagation for a plane wave of wavenumber $\boldsymbol{\beta}$, according to the numerical scheme of which $G_{\boldsymbol{\beta}}$ is an amplification factor. For the wave equation model problem, the speed of any plane wave solution will simply be γ, but the numerical phase velocity will in general be different, and in particular, wave speeds will be directionally dependent to a certain degree, depending on the type of scheme used. For all these schemes, the numerical phase velocity for at least one of the amplification factors will approach

the correct physical velocity near the spatial DC frequency, by *consistency* of the numerical scheme with the wave equation[2].

3 Finite Difference Schemes for the (2+1)D Wave Equation

Waveguide meshes of rectilinear [10], interpolated rectilinear [4], triangular [4, 11] and hexagonal [11] forms have all been applied to solve the (2+1)D wave equation. Though they have often been written as scattering forms, we showed in Chapter 4 of [2] that such meshes can also be written as finite difference schemes. There are quite a few computational issues that arise which serve to distinguish between these difference schemes. Among them are the density of grid points, the possibility of decomposing a given scheme into more computationally efficient subschemes, the operation count, spectral characteristics, the ease with which boundary conditions can be implemented, as well as the maximum allowable time step. The stability issue discussed in §2.2 may also be a concern, and thus favor a waveguide mesh implementation instead of a straightforward difference scheme. It is, of course, impossible to say which is best, without knowing problem specifics. The following is intended partly as a catalogue, as well as an indication of certain features which probably deserve more attention, in particular the distinction between passivity and stability which becomes apparent in the cases of the triangular and interpolated meshes.

It is worthwhile introducing two new quantities at this point. In addition to Δ, the "nearest-neighbor" grid spacing, or inter-junction spacing, T the time step, v_0, which will always be equal to Δ/T, and $\lambda = \gamma/v_0$, we also define ρ_S, the *computational density* of a particular scheme S to be number of grid points at which the the difference scheme is operative, per unit volume and per unit time. Thus if the N-dimensional volume of the spatial domain $\mathcal{D}$ of a particular problem is $|\mathcal{D}|$ and the total time over which it operates is $\mathcal{T}$, then the total number of grid point calculations which will need to be made will be $|\mathcal{D}|\mathcal{T}\rho_S$. Similarly, we can define the *add density* σ_S to be $A_S\rho_S$ if scheme S requires A_S adds in order to update at any given grid point. A multiply density could be defined similarly, though we will not, for reasons of space, do so here.

3.1 The Rectilinear Scheme

The finite difference scheme corresponding to a rectilinear mesh is obtained by applying centered differences to the wave equation, over a rectangular grid with indices i and j (which refer to points with spatial coordinates $x = i\Delta$ and $y = j\Delta$). The difference scheme is (see Equation (4.53) of [2])

$$\begin{aligned} U_{i,j}(n+1) + U_{i,j}(n-1) = \lambda^2\Big(U_{i+1,j}(n) + U_{i-1,j}(n) + U_{i,j+1}(n) + U_{i,j-1}(n)\Big) \\ + \left(2 - 4\lambda^2\right) U_{i,j}(n) \end{aligned} \tag{13}$$

and the amplification polynomial equation is of the form (5), with

$$B_{\boldsymbol{\beta}} = -2\Big(1 + \lambda^2\left(\cos(\beta_x\Delta) + \cos(\beta_y\Delta) - 2\right)\Big)$$

[2]Regrettably, a full discussion of consistency of difference schemes would take us too far afield, and we refer to [8] for a full exposition. The idea, grossly speaking, is that for a stable difference scheme, consistency is our guarantee that the numerical solution to the difference scheme converges to the solution of the continuous model problem as the grid spacing and time step are decreased. It is usually checked via a Taylor expansion of the difference scheme.

for $\boldsymbol{\beta} = [\beta_x, \beta_y]^T$. From (7), we thus have

$$F_{\boldsymbol{\beta}} = \cos(\beta_x \Delta) + \cos(\beta_y \Delta) - 2$$

and we have

$$\max_{\boldsymbol{\beta}} F_{\boldsymbol{\beta}} = 0 \qquad \min_{\boldsymbol{\beta}} F_{\boldsymbol{\beta}} = -4$$

Condition (8) is thus satisfied, and condition (9) gives the bound

$$\lambda \leq \frac{1}{\sqrt{2}} \qquad \text{for stability}$$

which implies that the amplification factor $|G_{\boldsymbol{\beta},\pm}| = 1$ for such values of λ. Because $\lambda = \gamma / v_0$, this bound is the same as the bound for passivity of the associated mesh scheme, given in (4.63) of [2]. The amplification factors, however, are distinct at all spatial frequencies only for $\lambda < 1/\sqrt{2}$. If $\lambda = 1/\sqrt{2}$, then the factors are degenerate for $\beta_x = \beta_y = 0$, and for $\beta_x = \beta_y = \pm\pi/\Delta$ and we are then in the situation discussed in §2.2 where linear growth of the solution may occur. This is an important special case, because it corresponds to the standard finite difference scheme for the rectilinear waveguide mesh (i.e. the realization without self-loops). The waveguide mesh implementation does not allow such growth at these frequencies[2]. As far as assessing the

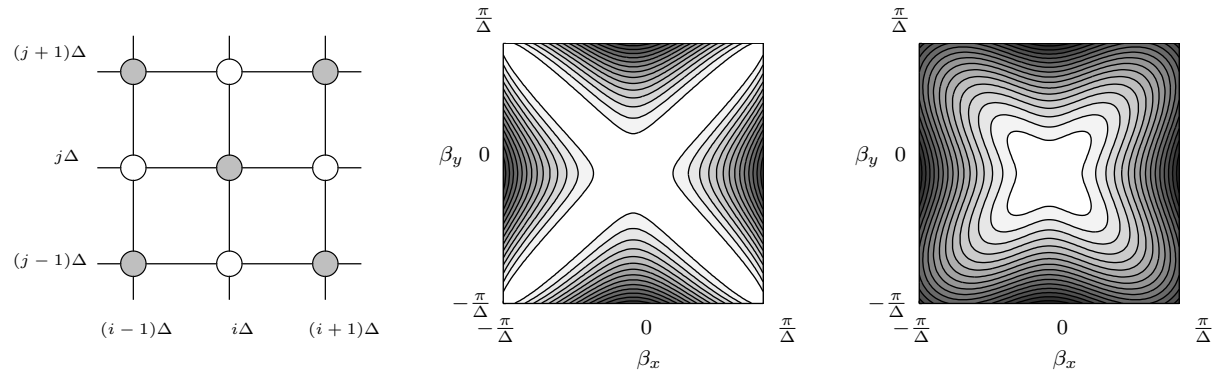

(a) (b) (c)

Figure 1: *The rectilinear scheme* (13)— (a) *grid, of spacing* Δ*, where grey/white coloring indicates a subgrid decomposition possible when* $\lambda = 1/\sqrt{2}$*.* (b) $v_{\boldsymbol{\beta},phase}/\gamma$ *for* $\lambda = 1/\sqrt{2}$*. Contour lines are drawn, representing successive deviations of 2 per cent from the ideal value of 1 which is obtained at spatial DC.* (c) $v_{\boldsymbol{\beta},phase}/\gamma$ *away from the stability bound, for* $\lambda = 1/2$*.*

computational requirements of the finite difference scheme, first consider the case $\lambda < 1/\sqrt{2}$. Five

[2]As an example of such growth at the spatial DC frequency, consider initializing the scheme (14) using $U_{i,j}(0) = 1$ for $i + j$ even and $U_{i,j}(1) = -1$ for $i + j$ odd. Then we will have $U_{i,j}(n) = 2n - 1$, for $i + j + n$ even. It is simple to show that a waveguide implementation does not allow us to choose bounded wave variable initial conditions which yield these values for $U_{i,j}(0)$ and $U_{i,j}(1)$.

adds are required at each grid point in order to update. Given that $T = \Delta/v_0$, we can write the computational and add densities for the scheme as

$$\rho_{rect} = \frac{v_0}{\Delta^3} \qquad \sigma_{rect} = \frac{5v_0}{\Delta^3} \qquad \text{for} \qquad v_0 > \sqrt{2}\gamma$$

For $\lambda = 1/\sqrt{2}$, however, scheme (13) simplifies to

$$U_{i,j}(n+1) + U_{i,j}(n-1) = \frac{1}{2}\Big(U_{i+1,j}(n) + U_{i-1,j}(n) + U_{i,j+1}(n) + U_{i,j-1}(n)\Big) \tag{14}$$

which may be operated on alternating grids, i.e., $U_{i,j}(n)$ need only be calculated for $i + j + n$ even (or odd). The computational and add densities, for $\lambda = 1/\sqrt{2}$ are then

$$\rho^s_{rect} = \frac{v_0}{2\Delta^3} \qquad \sigma^s_{rect} = \frac{2v_0}{\Delta^3} \qquad \text{for} \qquad v_0 = \sqrt{2}\gamma$$

where we note that the reduced scheme (14) requires only four adds for updating at a given grid point; in addition, the multiplies by 1/2 may be accomplished, in a fixed-point implementation, by simple bit-shifting operations. The increased efficiency of this scheme must be weighed against the danger of instability, and the fact that because grid density is reduced, the scheme is now applicable over a smaller range of spatial frequencies. The numerical phase velocities of the schemes, at the stability limit, and away from it, at $\lambda = 1/2$, are plotted in Figure 1. It is interesting to note that away from the stability limit, the numerical dispersion is somewhat less directionally dependent; this important factor may be useful from the point of view of frequency-warping techniques [4] which may be used to reduce numerical dispersion effects for schemes which are relatively directionally-independent. This idea has been discussed in the waveguide mesh context (where self-loops will be present) in [7].

3.2 The Interpolated Rectilinear Scheme

This scheme, like the standard rectilinear scheme, is defined over a grid with indices i and j, for points with $x = i\Delta$ and $y = j\Delta$. Updating, in this case, at a given point, requires access to values of the grid function at the previous time step at nearest-neighbor grid points to the north, east, west and south, as well as those to the north-east, north-west, south-east and south-west, which are more distant by a factor of $\sqrt{2}$. The scheme is referred to as "interpolated" in [4] because it is derived as an approximation to a hypothetical (and non-realizable) multi-directional difference scheme with minimally directionally-dependent numerical dispersion. (It is perhaps more useful to think of the scheme as interpolating between two rectilinear schemes operating on grids with a relative angle of 45 degrees.) The difference scheme will have the form

$$\begin{aligned} U_{i,j}(n+1) + U_{i,j}(n-1) = {} & \lambda^2 a\Big(U_{i,j+1}(n) + U_{i,j-1}(n) + U_{i+1,j}(n) + U_{i-1,j}(n)\Big) \\ & + \lambda^2 b\Big(U_{i+1,j+1}(n) + U_{i+1,j-1}(n) + U_{i-1,j+1}(n) + U_{i-1,j-1}(n)\Big) \\ & + \lambda^2 c U_{i,j}(n) \end{aligned} \tag{15}$$

for constants a, b and c which satisfy the constraints

$$a + 2b = 1 \qquad\qquad 4a + 4b + c = \frac{2}{\lambda^2} \tag{16}$$

for consistency with the wave equation. If $b = 0$, we get the standard rectilinear scheme, and if $a = 0$, we get a rectilinear scheme operating on a grid of spacing $\sqrt{2}\Delta$, which is rotated by 45 degrees with respect to that of the standard scheme. This general form was put forth in [4], and the free parameter a may be adjusted to give a less directionally dependent numerical phase velocity; it may thus be used in conjunction with frequency-warping methods for reducing dispersion error. In general, the interpolated scheme cannot be decomposed into mutually exclusive subschemes.

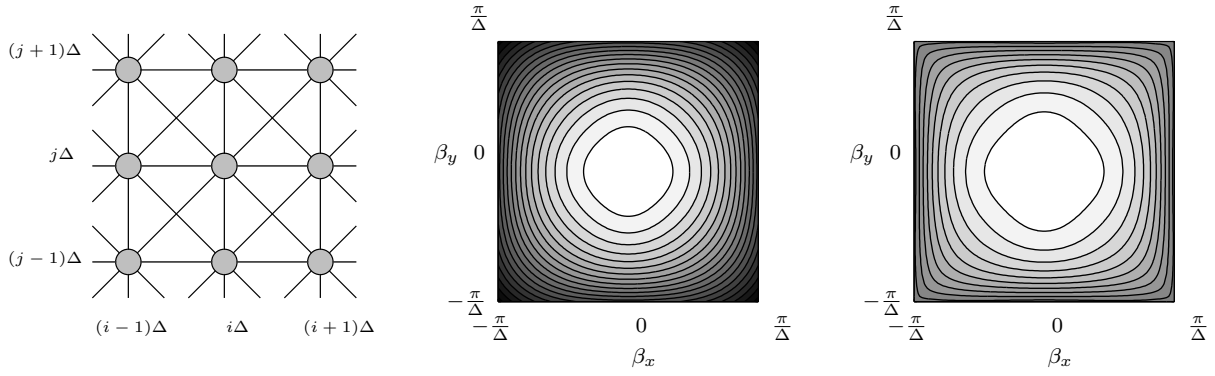

(a) (b) (c)

Figure 2: *The interpolated rectilinear scheme* (15)— (a) *numerical grid and connections for the interpolated rectilinear scheme* (15)*;* (b) $v_{\boldsymbol{\beta},phase}/\gamma$ *of the scheme for* $a = 0.62$ *at the "passivity" bound,* $\lambda = 1/\sqrt{1+a}$*;* (c) $v_{\boldsymbol{\beta},phase}/\gamma$ *for* $a = 0.62$*, at the stability bound, for* $\lambda = 1/\sqrt{2a}$*.*

It is possible to examine the stability of this method as in the previous case. We again have an amplification polynomial equation of the form of (5), with

$$B_{\boldsymbol{\beta}} = -2\lambda^2\Big(a(\cos(\beta_x\Delta) + \cos(\beta_y\Delta)) + (1-a)\cos(\beta_x\Delta)\cos(\beta_y\Delta) - 1 - a\Big) - 2$$

and thus

$$F_{\boldsymbol{\beta}} = a\big(\cos(\beta_x\Delta) + \cos(\beta_y\Delta)\big) + (1-a)\cos(\beta_x\Delta)\cos(\beta_y\Delta) - 1 - a$$

Note that $F_{\boldsymbol{\beta}}$ is *multilinear* [1] in $\cos(\beta_x\Delta)$ and $\cos(\beta_y\Delta)$, so that any extrema must occur at the corners of the region in the spatial frequency plane defined by $|\cos(\beta_x\Delta)| \le 1$, and $|\cos(\beta_y\Delta)| \le 1$. Thus, we need evaluate $F_{\boldsymbol{\beta}}$ only for $\boldsymbol{\beta}^T = [\beta_x, \beta_y] = [0,0]$, $[\pi/\Delta, 0]$, $[0, \pi/\Delta]$ and $[\pi/\Delta, \pi/\Delta]$:

$$F_{\boldsymbol{\beta}^T=[0,0]} = 0 \qquad F_{\boldsymbol{\beta}^T=[\pi/\Delta,0]} = F_{\boldsymbol{\beta}^T=[0,\pi/\Delta]} = -2 \qquad F_{\boldsymbol{\beta}^T=[\pi/\Delta,\pi/\Delta]} = -4a$$

The global maximum of $F_{\boldsymbol{\beta}}$ is non-positive (and thus condition (8) is satisfied) only if $a \ge 0$. The global minimum of $F_{\boldsymbol{\beta}}$, over this range of a will then be

$$\min_{\boldsymbol{\beta}} F_{\boldsymbol{\beta}} = \begin{cases} -2, & 0 \le a \le \frac{1}{2} \\ -4a, & a \ge \frac{1}{2} \end{cases}$$

and the stability bound on λ will be

$$\lambda \leq \begin{cases} 1, & 0 \leq a \leq \frac{1}{2} \\ \frac{1}{\sqrt{2a}}, & a \geq \frac{1}{2} \end{cases} \qquad \text{(for Von Neumann stability)} \tag{17}$$

It is interesting to look at the interpolated scheme from a waveguide mesh point of view (see Chapter 4 of [2] for details). At each grid point we will have a nine-port parallel scattering junction; four connections are made to neighboring points to the north, south, east and west, through a unit-delay bidirectional delay line of admittance Y_a, four more connections are made to the points to the north-east, south-east, north-west and south-west using waveguides of admittance Y_b, and there will be a self-loop of admittance Y_c. If the junction voltage is written as $U_{i,j}(n)$, then the difference scheme corresponding to this waveguide mesh will be exactly (15), with

$$\lambda^2 a = \frac{2Y_a}{Y_J} \qquad \lambda^2 b = \frac{2Y_b}{Y_J} \qquad \lambda^2 c = \frac{2Y_c}{Y_J}$$

where the junction admittance Y_J (assumed positive) will be given by

$$Y_J = 4Y_a + 4Y_b + Y_c$$

The passivity condition will then be a condition on the positivity of Y_a, Y_b and Y_c. From the previous discussion, we already require $a \geq 0$, so this ensures that $Y_a \geq 0$. Requiring $Y_b \geq 0$ is equivalent to requiring $b \geq 0$; from the first of constraints (16), this is true only for $a \leq 1$. Requiring $Y_c \geq 0$ is equivalent to requiring finally, from the second of constraints (16), that

$$\lambda \leq \frac{1}{\sqrt{1+a}}, \qquad 0 \leq a \leq 1 \qquad \text{(for passivity)}$$

The difference between the constraints for stability from (17) and the passivity constraint above is striking; these bounds are graphed in Figure 3. This is not the last time that we will find a

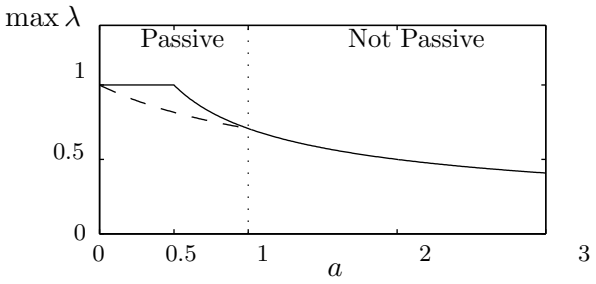

Figure 3: *Stability bounds for the interpolated rectilinear scheme, as a function of the free parameter a. The solid line indicates the maximum value of λ for a given value of a, and the dashed line the maximum value of λ allowed in a passive waveguide mesh implementation. Note that there is a passive realization only for $0 \leq a \leq 1$.*

discrepancy between Von Neumann stability of a scheme and passivity of the related mesh structure; it will come up again in the following section during a discussion of the triangular scheme, and in §4.3 when we look at the (3+1)D interpolated scheme. It is interesting to note that for a given

value of a, with $0 \leq a \leq 1$, the numerical dispersion properties can always be improved if we are willing to forego passivity (and a mesh implementation). We have plotted the numerical phase velocities of this scheme for $a = 0.62$, at both the stability limit and the passivity limit in Figure 2.

Finally, we mention that the computational and add densities for this scheme will be, in general,

$$\rho_{interp} = \frac{v_0}{\Delta^3} \qquad\qquad \sigma_{interp} = \frac{10v_0}{\Delta^3}$$

over the range of v_0 allowed by the stability constraint (17). For the scheme at the passivity bound (for $\lambda = 1/\sqrt{1+a}$, with $0 < a < 1$), we have

$$\rho^p_{interp} = \frac{\gamma\sqrt{1+a}}{\Delta^3} \qquad\qquad \sigma^p_{interp} = \frac{9\gamma\sqrt{1+a}}{\Delta^3}$$

We recall that for $a = 0$ or $a = 1$, at the stability limit, we again have the standard rectilinear scheme, for which a grid decomposition is possible; this was discussed in the previous section.

3.2.1 Optimally direction-independent numerical dispersion

Although the choice of the free parameter a which gives a maximally direction-independent numerical dispersion profile has been made, in the past, through computerized optimization procedures [4], we note here that it is possible to make a theoretical choice as well, based on a Taylor series expansion of the spectrum.

The spectral amplification factors for the interpolated scheme can be written in terms of the function $B_{\boldsymbol{\beta}}$, or, equivalently, in terms of the function $F_{\boldsymbol{\beta}}$. It should be clear, then, that if $F_{\boldsymbol{\beta}}$ is directionally independent, then so are the amplification factors, and thus the numerical phase velocity (see §2.4) as well. Ideally, we would like $F_{\boldsymbol{\beta}}$ to be a function of the spectral radius $\|\boldsymbol{\beta}\|_2 = (\beta_x^2 + \beta_y^2)^{1/2}$ alone. Now examine the Taylor expansion of $F_{\boldsymbol{\beta}}$ about $\boldsymbol{\beta} = \mathbf{0}$:

$$F_{\boldsymbol{\beta}} = -\Delta^2\|\boldsymbol{\beta}\|_2^2 + \Delta^4\left(\frac{1}{4!}\left(\beta_x^4 + \beta_y^4\right) + \frac{1-a}{4}\beta_x^2\beta_y^2\right) + O(\Delta^6)$$

The directionally-independent $O(\Delta^2)$ term reflects the fact that the scheme is consistent with the wave equation; higher order terms in general show directional dependence. The choice of $a = 2/3$, however, gives

$$F_{\boldsymbol{\beta}} = -\Delta^2\|\boldsymbol{\beta}\|_2^2 + \frac{1}{4!}\Delta^4\|\boldsymbol{\beta}\|_2^4 + O(\Delta^6) \qquad \text{for} \quad a = 2/3$$

and the directional dependence is confined to higher-order powers of Δ. Thus for this choice of a, the numerical scheme is maximally direction independent about spatial DC. Note that this value of a does fall within the required bounds for a passive waveguide mesh implementation. The value of 0.62 (for which the numerical dispersion profile is plotted in Figure 2), which is very close to 2/3, was chosen by visual inspection of dispersion profiles for various values of a.

3.3 The Triangular Scheme

The simplest difference scheme which can be used to solve the wave equation on a triangular grid, and which corresponds to the waveguide mesh discussed in [2] in the constant-coefficient case, is

given by

$$\begin{aligned} U_{i,j}(n+1) + U_{i,j}(n-1) = \frac{2}{3}\lambda^2 \Big(& U_{i,j+2}(n) + U_{i,j-2}(n) + U_{i+1,j+1}(n) + U_{i+1,j-1}(n) \\ & + U_{i-1,j+1}(n) + U_{i-1,j-1}(n) \Big) \\ & + 2\left(1 - 2\lambda^2\right) U_{i,j}(n) \end{aligned} \tag{18}$$

for a grid defined by points at indices (i, j), for integer i and j such that $i + j$ is even. These coordinates refer to grid points at locations $x = \sqrt{3}i\Delta/2$ and $y = j\Delta/2$, so that a given grid point is equidistant from its six neighbors. This arrangement is shown in Figure 4(a) and can be considered to be a rectilinear grid under a coordinate transformation; we refer to [9] for a discussion of the range of allowable spatial frequencies for such a grid.

In this case, we will again have an amplification polynomial of the form (5), with

$$\begin{aligned} B_{\boldsymbol{\beta}} &= -2\left(1 + \frac{2}{3}\lambda^2\left(\cos(\beta_y\Delta) + 2\cos(\frac{\beta_y\Delta}{2})\cos(\frac{\sqrt{3}\beta_x\Delta}{2}) - 3\right)\right) \\ F_{\boldsymbol{\beta}} &= \frac{2}{3}\left(\cos(\beta_y\Delta) + 2\cos(\frac{\beta_y\Delta}{2})\cos(\frac{\sqrt{3}\beta_x\Delta}{2}) - 3\right) \end{aligned}$$

Because $F_{\boldsymbol{\beta}}$ is not multilinear (see §3.2) in the cosines, finding the extrema is not as simple as in the interpolated case—one can proceed either through some tedious algebra, change to stretched rectilinear coordinates, in which $F_{\boldsymbol{\beta}}$ becomes multilinear again, or make use of a computer. In any case, these extrema can be shown to be

$$\max_{\boldsymbol{\beta}} F_{\boldsymbol{\beta}} = 0 \qquad\qquad \min_{\boldsymbol{\beta}} F_{\boldsymbol{\beta}} = -3$$

and thus, from (9),

$$\lambda \leq \sqrt{\frac{2}{3}} \qquad\qquad \text{for stability}$$

This is surprising, because the bound for passivity, from Eqn. (4.80) of [2], of the triangular mesh is $\lambda \leq 1/\sqrt{2}$. That is to say, for a given inter-junction spacing of Δ, a triangular waveguide mesh is concretely passive for time steps T with $T \leq \Delta/(\sqrt{2}\gamma)$. The corresponding difference equation, namely (18), is *stable* (in the sense of Von Neumann), for $T \leq \sqrt{2}\Delta/(\sqrt{3}\gamma)$. The waveguide mesh can of course operate in a non-passive mode for $1/\sqrt{2} < \lambda \leq \sqrt{2/3}$ (where we will require negative self-loop immittances, and will not have a simple positive definite energy measure for the network in terms of the wave quantities). The numerical dispersion characteristics of the scheme at the two bounds are considerably different, and are plotted in Figure 4(b) and (c); the phase velocities are near the correct physical velocity over a much wider range of spatial frequencies at the stability bound, though the dispersion is also more directional.

The question which arises here is of the distinction between passive and stable numerical methods (this was also seen for the mesh for the transmission line equations in the previous section on the interpolated rectilinear scheme). Is it always possible to find a passive realization of a stable numerical method? The discussion on the hexagonal mesh will help to answer this question. To this end, we note that at the stability limit, we can rewrite $B_{\boldsymbol{\beta}}$ as

$$B_{\boldsymbol{\beta}} = 2(1 - \frac{2}{9}|\psi_{\boldsymbol{\beta}}|^2) \qquad\qquad \text{for} \qquad \lambda = \sqrt{\frac{2}{3}}$$

for a function $\psi_{\boldsymbol{\beta}}$ whose squared magnitude is given by

$$|\psi_{\boldsymbol{\beta}}|^2 = 1 + 4\cos^2(\frac{\beta_y\Delta}{2}) + 4\cos(\frac{\beta_y\Delta}{2})\cos(\frac{\sqrt{3}\beta_x\Delta}{2})$$

The spectral amplification factors at the stability limit will then be, from (6),

$$G_{\boldsymbol{\beta},\pm} = -1 + \frac{2}{9}|\psi_{\boldsymbol{\beta}}|^2 \pm \frac{2}{3}|\psi_{\boldsymbol{\beta}}|\left(\frac{1}{9}|\psi_{\boldsymbol{\beta}}|^2 - 1\right)^{\frac{1}{2}} \tag{19}$$

For $\lambda = \sqrt{2/3}$ (its limiting value), the triangular scheme has the same potential for instability as the rectilinear scheme. Linear growth may occur for this scheme at the seven spatial frequency pairs

$$\boldsymbol{\beta}^T = [0,0], \quad [0, \pm 4\pi/3\Delta], \quad [2\pi/\sqrt{3}\Delta, \pm 2\pi/3\Delta], \quad [-2\pi/\sqrt{3}\Delta, \pm 2\pi/3\Delta]$$

The computational and add densities for the triangular scheme in general, and at the stability

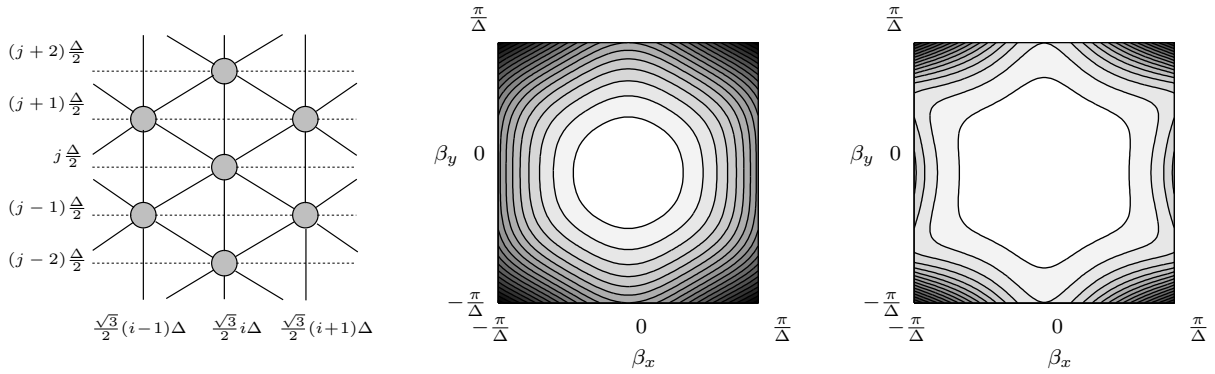

Figure 4: *The triangular scheme* (18)— (a) *numerical grid and connections;* (b) $v_{\boldsymbol{\beta},phase}/\gamma$ *for the scheme at the passivity bound,* $\lambda = 1/\sqrt{2}$*;* (c) $v_{\boldsymbol{\beta},phase}/\gamma$ *at the stability bound, for* $\lambda = \sqrt{2/3}$*.*

($\lambda = \sqrt{2/3}$) and passivity bounds ($\lambda = 1/\sqrt{2}$) will be

$$\rho_{tri} = \frac{2v_0}{\sqrt{3}\Delta^3} \qquad \sigma_{tri} = \frac{14v_0}{\sqrt{3}\Delta^3}$$
$$\rho^s_{tri} = \frac{\sqrt{2}\gamma}{\Delta^3} \qquad \sigma^s_{tri} = \frac{7\sqrt{2}\gamma}{\Delta^3}$$
$$\rho^p_{tri} = \frac{2\sqrt{2}\gamma}{\sqrt{3}\Delta^3} \qquad \sigma^p_{tri} = \frac{4\sqrt{6}\gamma}{\Delta^3}$$

Here we have taken into account the fact that at the passivity bound, we require one less add per point (in the waveguide mesh implementation, the self-loop disappears). We also mention

that the triangular difference scheme is doubly pathological, in the sense that not only do its passivity and stability regimes not coincide (and aside from the interpolated rectilinear schemes, it is the only scheme examined in this appendix that exhibits this behavior), but it also can not be decomposed into even/odd mutually exclusive subschemes, as can all the other schemes to be discussed here (again, excepting the interpolated scheme). It seems reasonable to conjecture that these two "symptoms" are related (somehow).

3.4 The Hexagonal Scheme

The hexagonal scheme is different from those previously discussed in that updating is not the same at every point on the grid. Indeed, one-half the grid points have a "mirror-image" orientation with respect to the other half, as shown in Figure 5(a). For this reason, we will take special care in the analysis of this system; first suppose that we have two grid functions $U_1(n)$ and $U_2(n)$ defined over the two sub grids (labelled 1 and 2, in Figure 5). We index these two grid functions as $U_{1,i,j}(n)$ and $U_{2,i+2,j}(n)$, for i and j integer such that $i = 3m$, for integer m, and $j + i/3$ is even. $U_{1,i,j}(n)$ will serve as an approximation to some continuous function u_1 at the point $(x = \Delta i/2, y = \sqrt{3}j\Delta/2, t = nT)$, and $U_{2,i+2,j}(n)$ will approximate a function u_2 at a point with coordinates $(x = \Delta i/2 + \Delta, y = \sqrt{3}j\Delta/2, t = nT)$. As before the distance between any grid point and its nearest neighbors (three in this case) is Δ. The difference scheme for the hexagonal waveguide mesh can then be written as the system

$$\begin{aligned} U_{1,i,j}(n+1) + U_{1,i,j}(n-1) &= \frac{4}{3}\lambda^2\Big(U_{2,i+2,j}(n) + U_{2,i-1,j+1}(n) + U_{2,i-1,j-1}(n)\Big) \\ &\quad +2\left(1-2\lambda^2\right)U_{1,i,j}(n) \qquad (20a) \\ U_{2,i+2,j}(n+1) + U_{2,i+2,j}(n-1) &= \frac{4}{3}\lambda^2\Big(U_{1,i,j}(n) + U_{1,i+3,j+1}(n) + U_{1,i+3,j-1}(n)\Big) \\ &\quad +2\left(1-2\lambda^2\right)U_{2,i+2,j}(n) \qquad (20b) \end{aligned}$$

Consistency of (20) with the wave equation is not immediately apparent. We can check it as follows. First expand (20) in a Taylor series in terms of the continuous functions u_1 and u_2 to get

$$\left(T^2\frac{\partial^2}{\partial t^2} + 4\lambda^2\right)u_1 = \lambda^2\left(4 + \Delta^2\nabla^2\right)u_2$$
$$\left(T^2\frac{\partial^2}{\partial t^2} + 4\lambda^2\right)u_2 = \lambda^2\left(4 + \Delta^2\nabla^2\right)u_1$$

to $O(\Delta^4, T^4)$. This system can then be reduced to

$$\left(T^2\frac{\partial^2}{\partial t^2} + 4\lambda^2\right)^2 u = \lambda^4\left(4 + \Delta^2\nabla^2\right)^2 u$$

where u is either of u_1 or u_2. Discarding higher order terms in T and Δ gives the wave equation.

In terms of the spatial Fourier spectra of the grid functions U_1 and U_2, we may write the differencing system (20) in the vector form of (10) with

$$\hat{\mathbf{U}}_{\boldsymbol{\beta}} = \begin{bmatrix}\hat{U}_{1,\boldsymbol{\beta}} \\ \hat{U}_{2,\boldsymbol{\beta}}\end{bmatrix} \qquad \mathbf{B}_{\boldsymbol{\beta}} = \begin{bmatrix}-2(1-2\lambda^2) & -\frac{4}{3}\lambda^2\psi_{\boldsymbol{\beta}} \\ -\frac{4}{3}\lambda^2\psi^*_{\boldsymbol{\beta}} & -2(1-2\lambda^2)\end{bmatrix}$$

where

$$\psi_{\boldsymbol{\beta}} = e^{i\beta_x \Delta} + 2e^{-i\beta_x \Delta/2} \cos(\sqrt{3}\beta_y \Delta/2)$$

Because $\mathbf{B}_{\boldsymbol{\beta}}$ is Hermitian, we can then change variables so that the system is the form of (11), with

$$\mathbf{\Lambda}_{\boldsymbol{\beta}} = \begin{bmatrix} -2(1-2\lambda^2) + \frac{4}{3}\lambda^2|\psi_{\boldsymbol{\beta}}| & 0 \\ 0 & -2(1-2\lambda^2) - \frac{4}{3}\lambda^2|\psi_{\boldsymbol{\beta}}| \end{bmatrix}$$

The necessary stability condition, from (12) will then be

$$\max_{\boldsymbol{\beta}} | -2(1-2\lambda^2) \pm \frac{4}{3}\lambda^2|\psi_{\boldsymbol{\beta}}|| \leq 2 \tag{21}$$

It is easy to check that $|\psi_{\boldsymbol{\beta}}|$ takes on a maximum of 3 when $\beta_x = \beta_y = 0$, and is minimized for $\beta_x = 0$, $|\beta_y| = 4\pi/(3\sqrt{3}\Delta)$ and for $|\beta_x| = 2\pi/3$, $|\beta_y| = 2\pi/(3\sqrt{3}\Delta)$, where it takes on the value 0. It is then easy to show that we require $\lambda \leq 1/\sqrt{2}$ in order to satisfy (21). This coincides with the passivity bound, from Eqn. (4.79) of [2].

An analysis of numerical dispersion is more complex in the vector case. Beginning from the uncoupled system defined by $\mathbf{\Lambda}_{\boldsymbol{\beta}}$, whose upper and lower diagonal entries we will call $\Lambda_{\boldsymbol{\beta},1}$ and $\Lambda_{\boldsymbol{\beta},2}$ respectively, we can see that we will thus have two pairs of spectral amplification factors, one for each uncoupled scalar equation. These will be given by

$$G_{\boldsymbol{\beta},1,\pm} = \frac{1}{2}\left(-\Lambda_{\boldsymbol{\beta},1} \pm \sqrt{\Lambda_{\boldsymbol{\beta},1}^2 - 4}\right) \qquad G_{\boldsymbol{\beta},2,\pm} = \frac{1}{2}\left(-\Lambda_{\boldsymbol{\beta},2} \pm \sqrt{\Lambda_{\boldsymbol{\beta},2}^2 - 4}\right)$$

It is useful to check the values of the amplification factors at the spatial DC frequency, and at the stability bound, where we have $\Lambda_{\boldsymbol{\beta},1} = 2$, $\Lambda_{\boldsymbol{\beta},2} = -2$. At this frequency, the spectral amplification factors take on the values

$$G_{\boldsymbol{\beta}=0,1,\pm} = -1 \qquad G_{\boldsymbol{\beta}=0,2,\pm} = 1 \tag{22}$$

Clearly, the pair of spectral amplification factors $G_{\boldsymbol{\beta}=0,2,\pm}$ correctly represents wave propagation at spatial DC, but the factors $G_{\boldsymbol{\beta}=0,1,\pm}$ will be responsible for *parasitic oscillations* [8] in the hexagonal scheme; they will not, in general, be overly problematic, since the energy allowed into such modes must vanish as the grid spacing Δ is decreased; this is a result of the consistency of the numerical scheme (20) with the wave equation, as was shown earlier in this subsection. In order to clarify this point, it is useful to examine the diagonalizing transformation defined by $\mathbf{J}_{\boldsymbol{\beta}}$, which takes the Fourier-transformed hexagonal scheme in the form of (10), in the variable $\hat{\mathbf{U}}_{\boldsymbol{\beta}}$, to that of (11), in $\hat{\mathbf{V}}_{\boldsymbol{\beta}}$. At $\boldsymbol{\beta} = 0$, and for $\lambda = 1/\sqrt{2}$, we have

$$\mathbf{B}_{\boldsymbol{\beta}=0} = \begin{bmatrix} 0 & -2 \\ -2 & 0 \end{bmatrix} \qquad \mathbf{\Lambda}_{\boldsymbol{\beta}=0} = \begin{bmatrix} 2 & 0 \\ 0 & -2 \end{bmatrix} \qquad \mathbf{J}_{\boldsymbol{\beta}=0} = \frac{1}{\sqrt{2}}\begin{bmatrix} -1 & 1 \\ 1 & 1 \end{bmatrix}$$

and thus $\hat{V}_{1,\boldsymbol{\beta}=0} = (-\hat{U}_{1,\boldsymbol{\beta}=0} + \hat{U}_{2,\boldsymbol{\beta}=0})/\sqrt{2}$ and $\hat{V}_{2,\boldsymbol{\beta}=0} = (\hat{U}_{1,\boldsymbol{\beta}=0} + \hat{U}_{2,\boldsymbol{\beta}=0})/\sqrt{2}$. Because scheme (20) is consistent with the wave equation, then for any reasonable choice of initial conditions, we must have that $\hat{U}_{1,\boldsymbol{\beta}=0} \approx \hat{U}_{2,\boldsymbol{\beta}=0}$, as Δ becomes small. Thus $\hat{V}_{1,\boldsymbol{\beta}=0}$, the component of the numerical solution whose spectral amplification is governed by the parasitic factor $G_{\boldsymbol{\beta}=0,1,\pm}$ must vanish in this limit as well.

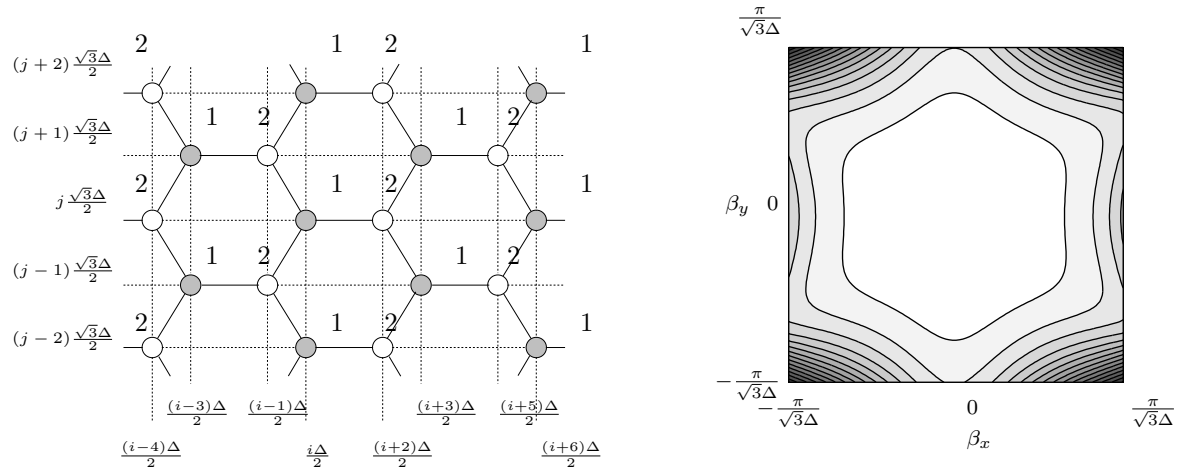

(a) (b)

Figure 5: *The hexagonal scheme* (20)— (a) *numerical grid and connections, where grey/white coloration of points indicates a division into mutually exclusive sub schemes at the stability bound;* (b) $v_{\boldsymbol{\beta},phase}/\gamma$ *for the scheme at the passivity bound,* $\lambda = 1/\sqrt{2}$*, for the dominant mode.*

The computational and add densities, for the general scheme (20), and at the stability limit for $\lambda = 1/\sqrt{2}$ will be given by

$$\rho_{hex} = \frac{4v_0}{3\sqrt{3}\Delta^3} \qquad \sigma_{hex} = \frac{16v_0}{3\sqrt{3}\Delta^3}$$

$$\rho^s_{hex} = \frac{2\sqrt{2}\gamma}{3\sqrt{3}\Delta^3} \qquad \sigma^s_{hex} = \frac{2\sqrt{2}\gamma}{\sqrt{3}\Delta^3}$$

As in the rectilinear scheme, we have used the fact that the hexagonal scheme decouples into two independent subschemes at the stability limit.

One other point is worthy of comment. Consider again the vector equation which describes the time evolution of the spatial spectra for the hexagonal scheme, which, in diagonalized form, is exactly (11). At the stability limit, then, for $\lambda = 1/\sqrt{2}$, we will have

$$\mathbf{\Lambda}_{\boldsymbol{\beta}} = \begin{bmatrix} \frac{2}{3}|\psi_{\boldsymbol{\beta}}| & 0 \\ 0 & -\frac{2}{3}|\psi_{\boldsymbol{\beta}}| \end{bmatrix}$$

Let us examine the second uncoupled subsystem. From (22), the spectral amplification factors will then be

$$G_{\boldsymbol{\beta},2,\pm} = \frac{1}{3}|\psi_{\boldsymbol{\beta}}| \pm \left(\frac{1}{9}|\psi_{\boldsymbol{\beta}}|^2 - 1\right)^{\frac{1}{2}}$$

It is of interest to see the effect of the amplification factors after *two* time steps; these will simply be the squares of $G_{\boldsymbol{\beta},2,\pm}$, which are

$$G^2_{\boldsymbol{\beta},2,\pm} = -1 + \frac{2}{9}|\psi_{\boldsymbol{\beta}}|^2 \pm \frac{2}{3}|\psi_{\boldsymbol{\beta}}| \left(\frac{1}{9}|\psi_{\boldsymbol{\beta}}|^2 - 1\right)^{\frac{1}{2}} \tag{23}$$

The important point here is that the *two-step* spectral amplification factors for scheme (20) are identical to the one-step factor for the triangular scheme with grid spacing $\sqrt{3}\Delta$ at its own stability limit; these factors were given in (19). This is perhaps not surprising, given that, from Figure 5(a), it is clear that that either of the two sub grids for the hexagonal scheme forms a triangular grid of spacing $\sqrt{3}\Delta$. What is surprising is that a triangular waveguide mesh at the stability limit is *not a concretely passive structure* (see previous section). That is to say, it will still operate stably (in the Von Neumann sense), but will require negative self-loop immittances. Thus a hexagonal waveguide mesh, at its passivity/stability bound can be seen as a *passive realization* of the stable difference scheme on a triangular grid. The question as to whether there is always a passive realization for any stable difference scheme remains open[2].

3.5 A Fourth-order Scheme

The schemes examined so far have all been spatially accurate to second-order. That is, at any time step, the L_2 norm of the difference between the numerical solution and the solution to the model problem will be proportional to Δ^2. In this section, we examine a family of explicit two-step schemes which are fourth-order spatially accurate. This family is more computationally intensive, due to the fact that updating the grid function requires access to past values which are two grid points away; in addition, we will see that a passive waveguide mesh implementation will not be possible in this case. These disadvantages are mitigated by the fact that the numerical dispersion is greatly reduced, so that the use of a coarse grid may be possible.

This scheme is, like the standard rectilinear scheme, defined over a grid with indices i and j which refer to a location with coordinates $x = i\Delta$ and $y = j\Delta$. Updating, in this case, at a given point, requires access to values of the grid function at the previous time step at the set of 25 grid points which are located at most 2Δ away in either the x or y directions, as shown in Figure 7(a). The difference scheme will have the general form

$$\begin{aligned} U_{i,j}(n+1) + U_{i,j}(n-1) = {} & \lambda^2 a\big(U_{i,j+1}(n) + U_{i,j-1}(n) + U_{i+1,j}(n) + U_{i-1,j}(n)\big) \\ & + \lambda^2 b\big(U_{i+1,j+1}(n) + U_{i+1,j-1}(n) + U_{i-1,j+1}(n) + U_{i-1,j-1}(n)\big) \\ & + \lambda^2 c\big(U_{i+2,j}(n) + U_{i-2,j}(n) + U_{i,j+2}(n) + U_{i,j-2}(n)\big) \\ & + \lambda^2 d\big(U_{i+2,j+1}(n) + U_{i+2,j-1}(n) + U_{i-2,j+1}(n) + U_{i-2,j-1}(n) \\ & \qquad + U_{i+1,j+2}(n) + U_{i+1,j-2}(n) + U_{i-1,j+2}(n) + U_{i-1,j-2}(n)\big) \\ & + \lambda^2 e\big(U_{i+2,j+2}(n) + U_{i+2,j-2}(n) + U_{i-2,j+2}(n) + U_{i-2,j-2}(n)\big) \\ & + \lambda^2 f U_{i,j}(n) \end{aligned} \tag{24}$$

In order for (24) to approximate the wave equation, we first require that the constants a, b, c, d, e and f satisfy the constraints

$$a + 2b + 4c + 10d + 8e = 1 \qquad 4a + 4b + 4c + 8d + 4e + f = \frac{2}{\lambda^2} \tag{25}$$

Then, to ensure that the scheme is fourth-order spatially accurate, we additionally require

$$b + 8d + 16e = 0 \qquad a + 2b + 16c + 34d + 32e = 0 \tag{26}$$

[2]We consider this to be the single most important issue raised in this thesis.

We can then write all the parameters in terms of d, e and λ, as

$$\begin{aligned} a &= 14d + 32e + 4/3 && \text{(27a)} \\ b &= -8d - 16e && \text{(27b)} \\ c &= -2d - 2e - 1/12 && \text{(27c)} \\ f &= 2/\lambda^2 - 24d - 60e - 5 && \text{(27d)} \end{aligned}$$

These constraints are all arrived at through a tedious but straightforward Taylor series expansion of the scheme. As for the interpolated scheme discussed in §3.2, passivity is guaranteed by a simple positivity condition on the scheme parameters, in this case $a, \ldots, f$. From (27c), it should be clear that if $d \geq 0$ and $e \geq 0$, then we must necessarily have $c \leq -1/12$, and a passive waveguide mesh implementation for this scheme is ruled out. This is not to say that fourth-order spatially accurate DWNs do not exist; we showed, in [2] that such a network does exist, at least in the case of the (1+1)D transmission line system (the wave equation is a special case of this system). The conclusion is that the topology of the form discussed in this section does not permit a mesh realization, but there are other forms that do.

The amplification polynomial for this scheme is of the form of (5), with $B_{\boldsymbol{\beta}} = -2\lambda^2 F_{\boldsymbol{\beta}} - 2$ and

$$\begin{aligned} F_{\boldsymbol{\beta}} = (14d + 32e + 4/3)\big(\cos(\beta_x\Delta) + \cos(\beta_y\Delta)\big) + (-16d - 32e)\cos(\beta_x\Delta)\cos(\beta_y\Delta) \\ + (-2d - 2e - 1/12)\big(\cos(2\beta_x\Delta) + \cos(2\beta_y\Delta)\big) \\ + 2d\big(\cos(\beta_x\Delta)\cos(2\beta_y\Delta) + \cos(2\beta_x\Delta)\cos(\beta_y\Delta)\big) \\ + 2e\cos(2\beta_x\Delta)\cos(2\beta_y\Delta) - 12d - 30e - 5/2 \end{aligned}$$

In order to determine stability bounds, we are faced with finding the extrema of $F_{\boldsymbol{\beta}}$ in terms of the parameters d and e. Because $F_{\boldsymbol{\beta}}$ is not multilinear in the cosines, finding these extrema explicitly is a challenging problem.

Let us first simplify the class of difference schemes by looking for those which exhibit maximally direction-independent numerical dispersion. As in §3.2, we expand $F_{\boldsymbol{\beta}}$ in a Taylor series about $\boldsymbol{\beta} = \mathbf{0}$, to get

$$F_{\boldsymbol{\beta}} = -\frac{\Delta^2}{2}\|\boldsymbol{\beta}\|_2^2 + \Delta^6\Big(\frac{1}{180}\left(\beta_x^6 + \beta_y^6\right) - (d/2 + 2e)\left(\beta_x^2\beta_y^4 + \beta_x^4\beta_y^2\right)\Big) + O(\Delta^8)$$

The absence of a term in Δ^4 reflects the fourth-order accuracy of the scheme. If we choose $d/2+2e = -1/60$, however, we get

$$F_{\boldsymbol{\beta}} = -\frac{\Delta^2}{2}\|\boldsymbol{\beta}\|_2^2 + \frac{\Delta^6}{180}\|\boldsymbol{\beta}\|_2^6 + O(\Delta^8) \qquad \text{for} \quad d/2 + 2e = -1/60$$

and the scheme is direction-independent to sixth order in Δ.

Making use of this setting for e in terms of d, $F_{\boldsymbol{\beta}}$ now depends only on the free parameter d; through a computer analysis, it is possible to show that condition (8) is satisfied for $d > -0.134$. The upper bound on λ, from condition (9) is plotted as a function of d in Figure 6.

We have plotted a numerical dispersion profile in Figure 7(b). It is interesting to note that the maximum value of $v_{\boldsymbol{\beta},phase}/\gamma$ for this family of schemes would always appear to be slightly greater than 1, although the numerical phase velocity does indeed approach the physical velocity at spatial DC (as it will for any consistent scheme).

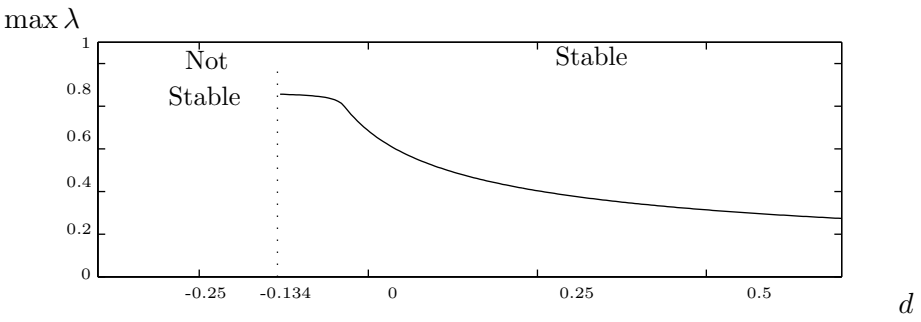

Figure 6: *Stability bound for the fourth-order scheme* (24)*, as a function of the free parameter d, in the optimally direction-independent case. The solid line indicates the maximum value of λ for a given value of d. The scheme is stable only for* $d > -0.134$.

The computational and add densities for this scheme are, in general,

$$\rho_{fourth} = \frac{v_0}{\Delta^3} \qquad\qquad \sigma_{fourth} = \frac{25 v_0}{\Delta^3}$$

There are several ways of cutting down on computational costs; for example, because d and e are free parameters, we may simply set them to zero, and the add density is significantly reduced. There is, however, no decomposition of this scheme into mutually exclusive subschemes.

4 Finite Difference Schemes for the (3+1)D Wave Equation

We now look at several difference schemes which solve the wave equation in (3+1)D, in particular schemes which operate on a rectilinear grid; all the schemes which have appeared in the DWN literature are of this type. We will pay special attention to the interpolated scheme, for which the requirements for stability and passivity become even more distinct than they were in the (2+1)D case (see §3.2).

4.1 The Cubic Rectilinear Scheme

This is the simplest scheme for the (3+1)D wave equation. The grid points, indexed by i, j and k are located at coordinates $(x, y, z) = (i\Delta, j\Delta, k\Delta)$. The finite difference scheme is written as

$$\begin{aligned} U_{i,j,k}(n+1) + U_{i,j,k}(n-1) = \lambda^2 \Big(& U_{i+1,j,k}(n) + U_{i-1,j,k}(n) + U_{i,j+1,k}(n) + U_{i,j-1,k}(n) \\ & + U_{i,j,k+1}(n) + U_{i,j,k-1}(n) \Big) \\ & + \left(2 - 6\lambda^2\right) U_{i,j,k}(n) \end{aligned} \tag{28}$$

If the grid points are located at the corners of a cubic lattice, then updating the scheme requires access to the grid function at the six neighboring corners; see Figure 8(a). The stability analysis is very similar to that of the (2+1)D rectilinear scheme, except that we now have a 3-tuple of spatial frequencies, $\boldsymbol{\beta} = [\beta_x, \beta_y, \beta_z]^T$. The amplification polynomial equation is again of the form of (5), with

$$B_{\boldsymbol{\beta}} = -2\left(1 + \lambda^2 \left(\cos(\beta_x \Delta) + \cos(\beta_y \Delta) + \cos(\beta_x \Delta) - 3\right)\right)$$

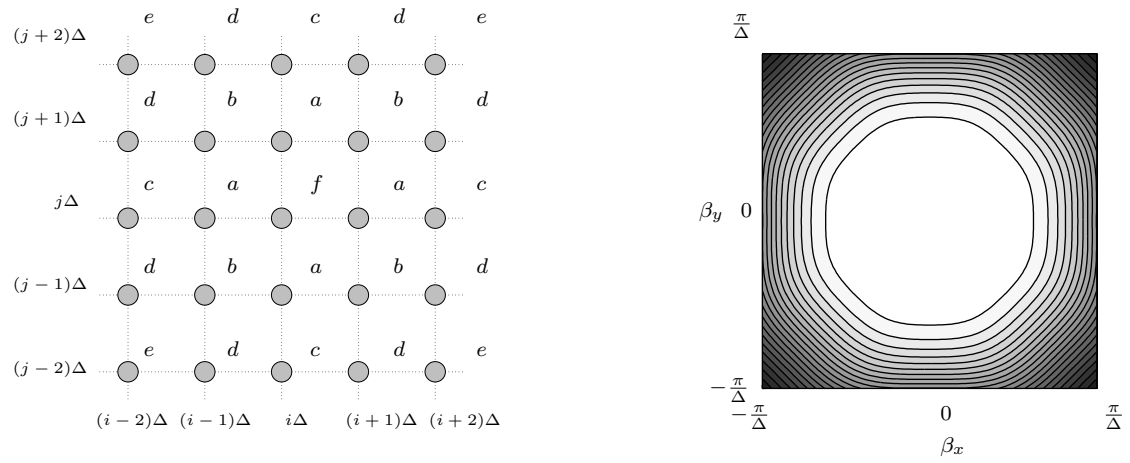

(a) (b)

Figure 7: *The fourth-order spatially accurate scheme* (24)— (a) *numerical grid, where the letters a through f refer to the related coefficients from* (24)*;* (b) $v_{\boldsymbol{\beta},phase}/\gamma$ *for the scheme at for* $d = -0.044$ *and* $\lambda = 0.6174$*, which is away from the bound shown in Figure 6.* $v_{\boldsymbol{\beta},phase}/\gamma$ *takes on a maximum of 1.0144 (not shown).*

and thus

$$F_{\boldsymbol{\beta}} = \cos(\beta_x\Delta) + \cos(\beta_y\Delta) + \cos(\beta_x\Delta) - 3$$

Because $F_{\boldsymbol{\beta}}$ is multilinear in the cosines, it is simple to show that

$$\max_{\boldsymbol{\beta}} F_{\boldsymbol{\beta}} = 0 \qquad \min_{\boldsymbol{\beta}} F_{\boldsymbol{\beta}} = -6$$

and so, from (9),

$$\lambda \leq \frac{1}{\sqrt{3}} \qquad \text{(for Von Neumann stability)}$$

When $\lambda = 1/\sqrt{3}$, the amplification factors become degenerate and linear growth of the solution may occur for $\beta_x = \beta_y = \beta_z = 0$, and for $|\beta_x| = |\beta_y| = |\beta_z| = \pi/\Delta$. The computational and add densities are

$$\rho_{cub} = \frac{v_0}{\Delta^4} \qquad \sigma_{cub} = \frac{7v_0}{\Delta^4}$$

for $v_0 > \sqrt{3}\gamma$, and

$$\rho^s_{cub} = \frac{\gamma}{2\Delta^4} \qquad \sigma^s_{cub} = \frac{3\gamma}{\Delta^4}$$

at the stability limit $v_0 = \sqrt{3}\gamma$. At this limit, the scheme may, like the (2+1)D scheme, be divided into two mutually exclusive subschemes. See Figure 8(b) and (c) for plots of the numerical dispersion properties of the cubic rectilinear scheme.

4.2 The Octahedral Scheme

The grid for an octahedral scheme is constructed from two superimposed rectilinear grids; if the points of the first grid are located at cube corners, then the points of the second will occur at the centers of the cubes defined by the first. The relevant difference scheme on an octahedral grid can be written as

$$\begin{aligned} U_{i,j,k}(n+1) + U_{i,j,k}(n-1) = \frac{3}{4}\lambda^2 \Big(& U_{i-1,j+1,k+1}(n) + U_{i+1,j+1,k+1}(n) + U_{i-1,j-1,k+1}(n) \\ & + U_{i+1,j-1,k+1}(n) + U_{i-1,j-1,k-1}(n) + U_{i-1,j+1,k-1}(n) \\ & + U_{i+1,j+1,k-1}(n) + U_{i+1,j-1,k-1}(n) \Big) \\ & + \left(2 - 8\lambda^2\right) U_{i,j,k}(n) \end{aligned} \tag{29}$$

for i, j and k which are either all even or all odd integers. Now, we have taken the spacing between nearest neighbors to be Δ, so the indices i, j and k refer to a point with coordinates $x = i\Delta/\sqrt{3}$, $y = j\Delta/\sqrt{3}$ and $z = k\Delta/\sqrt{3}$. The amplification polynomial equation is again of the form (5), with

$$B_{\boldsymbol{\beta}} = -2\left(1 + 3\lambda^2\left(\cos(\frac{\beta_x\Delta}{\sqrt{3}})\cos(\frac{\beta_y\Delta}{\sqrt{3}})\cos(\frac{\beta_x\Delta}{\sqrt{3}}) - 1\right)\right)$$

and

$$F_{\boldsymbol{\beta}} = 3\left(\cos(\frac{\beta_x\Delta}{\sqrt{3}})\cos(\frac{\beta_y\Delta}{\sqrt{3}})\cos(\frac{\beta_x\Delta}{\sqrt{3}}) - 1\right)$$

and it is again easy to determine that

$$\max_{\boldsymbol{\beta}} F_{\boldsymbol{\beta}} = 0 \qquad\qquad \min_{\boldsymbol{\beta}} F_{\boldsymbol{\beta}} = -6$$

which are the same as the bounds in the cubic rectilinear case. We again have that

$$\lambda \le \frac{1}{\sqrt{3}} \qquad\qquad \text{(for Von Neumann stability)}$$

Thus the stability bound coincides with the passivity bound for the mesh implementation. For $\lambda = 1/\sqrt{3}$, instabilities may appear at any spatial frequency triplets $\boldsymbol{\beta} = [\beta_x, \beta_y, \beta_z]^T$ where each component is either 0 or $\pm\sqrt{3}\pi/\Delta$.

The computational and add densities are given by

$$\rho_{oct} = \frac{3\sqrt{3}v_0}{4\Delta^4} \qquad\qquad \sigma_{oct} = \frac{27\sqrt{3}v_0}{4\Delta^4}$$

for $v_0 > \sqrt{3}\gamma$, and

$$\rho^s_{oct} = \frac{9\gamma}{8\Delta^4} \qquad\qquad \sigma^s_{oct} = \frac{9\gamma}{\Delta^4}$$

at the stability limit $v_0 = \sqrt{3}\gamma$.

At the stability limit, the scheme can be divided into two mutually exclusive subschemes; plots of numerical dispersion are shown in Figure 9(b) and (c). It is interesting to note that there is no dispersion error along the six axial directions; this should be compared with the cubic rectilinear scheme, for which wave propagation is dispersionless along the diagonal directions (there are eight such directions).

4.3 The (3+1)D Interpolated Rectilinear Scheme

In the interest of achieving a more uniform numerical dispersion profile in (3+1)D, it is of course possible to define an interpolated scheme, in the same way as was done in (2+1)D in §3.2. We will again have a two-step scheme, and updating at a given grid point is performed with reference to, at the previous time step, the grid point at the same location, as well as the 26 nearest neighbors: the six points a distance Δ away, twelve points at a distance of $\sqrt{2}\Delta$, and eight points that are $\sqrt{3}\Delta$ away (see Figure 11(a)). This (3+1)D rectilinear scheme has been discussed recently in [3, 5]; we present here a complete analysis of the relevant stability conditions, as well as the conditions under which a waveguide mesh implementation exists. We also look at a means of minimizing directional dependence of the numerical dispersion.

Like the cubic rectilinear and octahedral schemes, this scheme will be defined over a rectilinear grid indexed by i, j and k and will have the general form

$$\begin{aligned}
U_{i,j,k}(n+1) + U_{i,j,k}(n-1) = \quad & \lambda^2 a\Big(U_{i+1,j,k}(n) + U_{i-1,j,k}(n) + U_{i,j+1,k}(n) + U_{i,j-1,k}(n) \\
& \quad + U_{i,j,k+1}(n) + U_{i,j,k-1}(n)\Big) \\
& + \lambda^2 b\Big(U_{i+1,j+1,k}(n) + U_{i+1,j-1,k}(n) + U_{i-1,j+1,k}(n) + U_{i-1,j-1,k}(n) \\
& \quad + U_{i+1,j,k+1}(n) + U_{i-1,j,k+1}(n) + U_{i,j+1,k+1}(n) + U_{i,j-1,k+1}(n) \\
& \quad + U_{i+1,j,k-1}(n) + U_{i-1,j,k-1}(n) + U_{i,j+1,k-1}(n) + U_{i,j-1,k-1}(n)\Big) \\
& + \lambda^2 c\Big(U_{i+1,j+1,k+1}(n) + U_{i+1,j+1,k-1}(n) + U_{i-1,j-1,k+1}(n) \\
& \quad + U_{i-1,j-1,k-1}(n) + U_{i+1,j-1,k+1}(n) + U_{i+1,j-1,k-1}(n) \\
& \quad + U_{i-1,j+1,k+1}(n) + U_{i-1,j+1,k-1}(n)\Big) \\
& + \lambda^2 d U_{i,j}(n)
\end{aligned} \tag{30}$$

In order for scheme (30) to satisfy the wave equation, we require the constants a, b, c and d to satisfy the constraints

$$a + 4b + 4c = 1 \qquad\qquad 6a + 12b + 8c + d = \frac{2}{\lambda^2}$$

We can then rewrite

$$c = \frac{1 - a - 4b}{4} \qquad\qquad d = \frac{2}{\lambda^2} - 4a - 4b - 2 \tag{31}$$

and a family of difference schemes parametrized by a, b and λ results.

The stability analysis of this scheme proceeds along the same lines as that of the (2+1)D scheme, though as we shall see, the stability condition on the parameters a and b is considerably more complex. As before, we have an amplification polynomial of the form of (5), now with

$$\begin{aligned}
B_{\boldsymbol{\beta}} = -2\lambda^2\Big(& a\big(\cos(\beta_x\Delta) + \cos(\beta_y\Delta) + \cos(\beta_z\Delta)\big) \\
& + 2b\big(\cos(\beta_x\Delta)\cos(\beta_y\Delta) + \cos(\beta_x\Delta)\cos(\beta_z\Delta) + \cos(\beta_y\Delta)\cos(\beta_z\Delta)\big) \\
& + (1 - a - 4b)\cos(\beta_x\Delta)\cos(\beta_y\Delta)\cos(\beta_z\Delta) - 2a - 2b - 1\Big) - 2
\end{aligned}$$

and

$$\begin{aligned} F_{\boldsymbol{\beta}} = a\big(&\cos(\beta_x\Delta)+\cos(\beta_y\Delta)+\cos(\beta_z\Delta)\big) \\ &+ 2b\big(\cos(\beta_x\Delta)\cos(\beta_y\Delta)+\cos(\beta_x\Delta)\cos(\beta_z\Delta)+\cos(\beta_y\Delta)\cos(\beta_z\Delta)\big) \\ &+ (1-a-4b)\cos(\beta_x\Delta)\cos(\beta_y\Delta)\cos(\beta_z\Delta) - 2a - 2b - 1 \end{aligned}$$

Because $F_{\boldsymbol{\beta}}$ is again multilinear in the three cosines, its extrema can only occur at the eight corners of the cubic region defined by $|\cos(\beta_x\Delta)| \le 1$, $|\cos(\beta_y\Delta)| \le 1$ and $|\cos(\beta_z\Delta)| \le 1$. These extrema are

$$\begin{aligned} F_{\boldsymbol{\beta}^T=[0,0,0]} &= 0 \\ F_{\boldsymbol{\beta}^T=[\pi/\Delta,0,0]} = F_{\boldsymbol{\beta}^T=[0,\pi/\Delta,0]} = F_{\boldsymbol{\beta}^T=[0,0,\pi/\Delta]} &= -2 \\ F_{\boldsymbol{\beta}^T=[\pi/\Delta,\pi/\Delta,0]} = F_{\boldsymbol{\beta}^T=[\pi/\Delta,0,\pi/\Delta]} = F_{\boldsymbol{\beta}^T=[\pi/\Delta,\pi/\Delta,0]} &= -4a - 8b \\ F_{\boldsymbol{\beta}^T=[\pi/\Delta,\pi/\Delta,\pi/\Delta]} &= -4a + 8b - 2 \end{aligned}$$

The non-positivity requirement on $F_{\boldsymbol{\beta}}$ then amounts to requiring that these extreme values be non-positive. The resulting stability region in the (a, b) plane is shown in grey in Figure 10(a).

Assuming that a and b fall in this region, we then must have

$$\lambda^2 \le -2/\min_{\boldsymbol{\beta}} F_{\boldsymbol{\beta}}$$

The minimum value of $F_{\boldsymbol{\beta}}$ depends on a and b in a non-trivial way; referring to Figure 10(a), the stability domain can be divided into three regions, and in each there is a different closed form expression for the upper bound on λ. These bounds are given explicitly in the caption to Figure 10(a).

In order to examine the directional dependence of the dispersion error, we may expand $F_{\boldsymbol{\beta}}$ in a Taylor series about $\boldsymbol{\beta}= \mathbf{0}$, as was done in the (2+1)D case. We have

$$F_{\boldsymbol{\beta}} = -\Delta^2\|\boldsymbol{\beta}\|_2^2 + \Delta^4\Big(\frac{1}{4!}\left(\beta_x^4+\beta_y^4+\beta_z^4\right) + \frac{1-a-2b}{4}\left(\beta_x^2\beta_y^2+\beta_x^2\beta_z^2+\beta_y^2\beta_z^2\right)\Big) + O(\Delta^6)$$

which implies that

$$F_{\boldsymbol{\beta}} = -\Delta^2\|\boldsymbol{\beta}\|_2^2 + \Delta^4\frac{1}{4!}\|\boldsymbol{\beta}\|_2^4 + O(\Delta^6) \qquad \text{for} \quad b = -a/2 + 1/3$$

and the dispersion error is directionally independent to fourth order. This special choice of the parameters a and b is plotted as a dotted line in Figure 10(a). It is well worth comparing this optimization method with the computer-based techniques applied to the same problem in [5].

The computational and add densities for the scheme will be

$$\rho_{3Dinterp} = \frac{v_0}{\Delta^4} \qquad\qquad \sigma_{3Dinterp} = \frac{27v_0}{\Delta^4}$$

Considerable computational savings are possible if any of a, b, c or d is zero. Finally, we remark that the (3+1)D interpolated scheme can be realized as a waveguide mesh, where, at any given junction, we will have four types of waveguide connections: those of admittances Y_a, Y_b and Y_c are connected to the neighboring junctions located at gridpoints at distances Δ, $\sqrt{2}\Delta$ and $\sqrt{3}\Delta$ away

respectively, and a self-loop of admittance Y_d is also connected to every junction. We end up with exactly difference scheme (30), with

$$\lambda^2 a = \frac{2Y_a}{Y_J} \qquad \lambda^2 b = \frac{2Y_b}{Y_J} \qquad \lambda^2 c = \frac{2Y_c}{Y_J} \qquad \lambda^2 d = \frac{2Y_d}{Y_J}$$

where the junction admittance Y_J will be given by

$$Y_J = 6Y_a + 12Y_b + 8Y_c + Y_d$$

The passivity condition is then a positivity condition on these admittances, and thus on the parameters a, b, c and d. Recalling the expression for c in terms of a and b from (31), we must have

$$a \geq 0 \quad b \geq 0 \quad b \leq \frac{1-a}{4}$$

This region is shown, in dark grey, in Figure 10(b). The positivity condition on d (expressed in terms of a, b and λ as per (31)) gives the bound on λ, which is

$$\lambda \leq \sqrt{\frac{1}{2a+2b+1}} \qquad \text{(for passivity)}$$

4.4 The Tetrahedral Scheme

The tetrahedral scheme in (3+1)D [11] is somewhat similar to the hexagonal scheme in (2+1)D, in that the grid is divided evenly into two sets of points, at which updating is performed using "mirror-image" stencils. It is different, however, because grid points can easily be indexed with reference to a regular cubic lattice; the hexagonal scheme operates on a rectangular grid in stretched or transformed coordinates. In fact, a tetrahedral scheme can be obtained directly from an octahedral scheme simply by removing half of the grid points it employs; as such, any given grid point in the tetrahedral scheme has four nearest neighbors. As usual, we assume the nearest-neighbor grid spacing to be Δ. See Figure 12(a) for a representation of the numerical grid.

As per the hexagonal scheme, we will view this as a vectorized scheme operating on two distinct sub grids, labelled 1 and 2 in Figure 12(a). The two grid functions $U_{1,i,j,k}(n)$ and $U_{2,i+1,j+1,k+1}(n)$ are defined for integers i, j and k all even such that $(i+j+k)/2$ is also even. $U_{1,i,j,k}$ will be used to approximate a continuous function u_1 at the point with coordinates $x = i\Delta/\sqrt{3}$, $y = j\Delta/\sqrt{3}$ and $z = k\Delta/\sqrt{3}$, and $U_{2,i+1,j+1,k+1}$ approximates u_2 at coordinates $x = (i+1)\Delta/\sqrt{3}$, $y = (j+1)\Delta/\sqrt{3}$ and $z = (k+1)\Delta/\sqrt{3}$. The numerical scheme can then be written as

$$\begin{aligned} U_{1,i,j,k}(n+1) + U_{1,i,j,k}(n-1) &= \frac{3}{2}\lambda^2\Big(U_{2,i+1,j+1,k+1}(n) + U_{2,i+1,j-1,k-1}(n) \\ &\qquad + U_{2,i-1,j-1,k+1}(n) + U_{2,i-1,j+1,k-1}(n)\Big) \\ &\quad + 2\left(1-3\lambda^2\right) U_{1,i,j,k}(n) \qquad (32a) \\ U_{2,i+1,j+1,k+1}(n+1) + U_{2,i+1,j+1,k+1}(n-1) &= \frac{3}{2}\lambda^2\Big(U_{1,i,j,k}(n) + U_{1,i,j+2,k+2}(n) \\ &\qquad + U_{1,i+2,j+2,k}(n) + U_{1,i+2,j,k+2}(n)\Big) \\ &\quad + 2\left(1-3\lambda^2\right) U_{2,i+1,j+1,k+1}(n) \qquad (32b) \end{aligned}$$

As for the hexagonal scheme, we may check consistency of this system with the wave equation by treating the grid functions as samples of continuous functions u_1 and u_2 and expanding (32) in terms of partial derivatives; both grid functions updated according to this scheme will approximate the solution to the wave equation on their respective grids.

Determining the stability condition proceeds as in the hexagonal scheme; taking spatial Fourier transforms of (32) gives a vector spectral update equation of the form (10), with $\mathbf{B}_{\boldsymbol{\beta}}$ given by

$$\mathbf{B}_{\boldsymbol{\beta}} = \begin{bmatrix} -2(1-3\lambda^2) & -\frac{3}{2}\lambda^2\psi_{\boldsymbol{\beta}} \\ -\frac{3}{2}\lambda^2\psi^*_{\boldsymbol{\beta}} & -2(1-3\lambda^2) \end{bmatrix}$$

with

$$\psi_{\boldsymbol{\beta}} = 2\Big(e^{j\Delta\beta_x/\sqrt{3}}\cos(\Delta(\beta_y+\beta_z)/\sqrt{3}) + e^{-j\Delta\beta_x/\sqrt{3}}\cos(\Delta(\beta_y-\beta_z)/\sqrt{3})\Big)$$

$\mathbf{B}_{\boldsymbol{\beta}}$ is again Hermitian, and has eigenvalues

$$\begin{aligned} \Lambda_{\boldsymbol{\beta},1} &= -2\left(1-3\lambda^2\right) + \frac{3}{2}\lambda^2|\psi_{\boldsymbol{\beta}}| \\ \Lambda_{\boldsymbol{\beta},2} &= -2\left(1-3\lambda^2\right) - \frac{3}{2}\lambda^2|\psi_{\boldsymbol{\beta}}| \end{aligned}$$

The stability condition can thus be written as

$$\left|-2\left(1-3\lambda^2\right) \pm \frac{3}{2}\lambda^2|\psi_{\boldsymbol{\beta}}|\right| \leq 2 \tag{33}$$

$\psi_{\boldsymbol{\beta}}$ can be shown to take on a maximum of 4, and a minimum of 0, and it then follows that (33) will be satisfied if and only if $\lambda \leq 1/\sqrt{3}$, the same bound as obtained for the cubic rectilinear and octahedral schemes. The bound is the same as the bound for passivity of a tetrahedral mesh. We note that as for these other schemes, the grid permits a subdivision into mutually exclusive subschemes at this stability limit—see Figure 12(a). By a simple comparison with the hexagonal scheme, we can obtain the four spectral amplification factors by

$$G_{\boldsymbol{\beta},1,\pm} = \frac{1}{2}\left(-\Lambda_{\boldsymbol{\beta},1} \pm \sqrt{\Lambda^2_{\boldsymbol{\beta},1}-4}\right) \qquad G_{\boldsymbol{\beta},2,\pm} = \frac{1}{2}\left(-\Lambda_{\boldsymbol{\beta},2} \pm \sqrt{\Lambda^2_{\boldsymbol{\beta},2}-4}\right)$$

it is easy to see that parasitic modes (characterized by the amplification factors $G_{\boldsymbol{\beta},1,\pm}$) will be present in the tetrahedral scheme, due to the nonuniformity of updating on the numerical grid. The numerical dispersion characteristics of the dominant modes with amplification factors $G_{\boldsymbol{\beta},2,\pm}$ are shown in planar and spherical cross-sections in Figure 12(b) and (c).

The computational and add densities of this scheme, in general, are

$$\rho_{tetr} = \frac{3\sqrt{3}v_0}{8\Delta^4} \qquad \sigma_{tetr} = \frac{15\sqrt{3}v_0}{8\Delta^4}$$

for $v_0 > \sqrt{3}\gamma$, and

$$\rho^s_{tetr} = \frac{9\gamma}{16\Delta^4} \qquad \sigma^s_{tetr} = \frac{9\gamma}{4\Delta^4}$$

at the stability limit $v_0 = \sqrt{3}\gamma$.

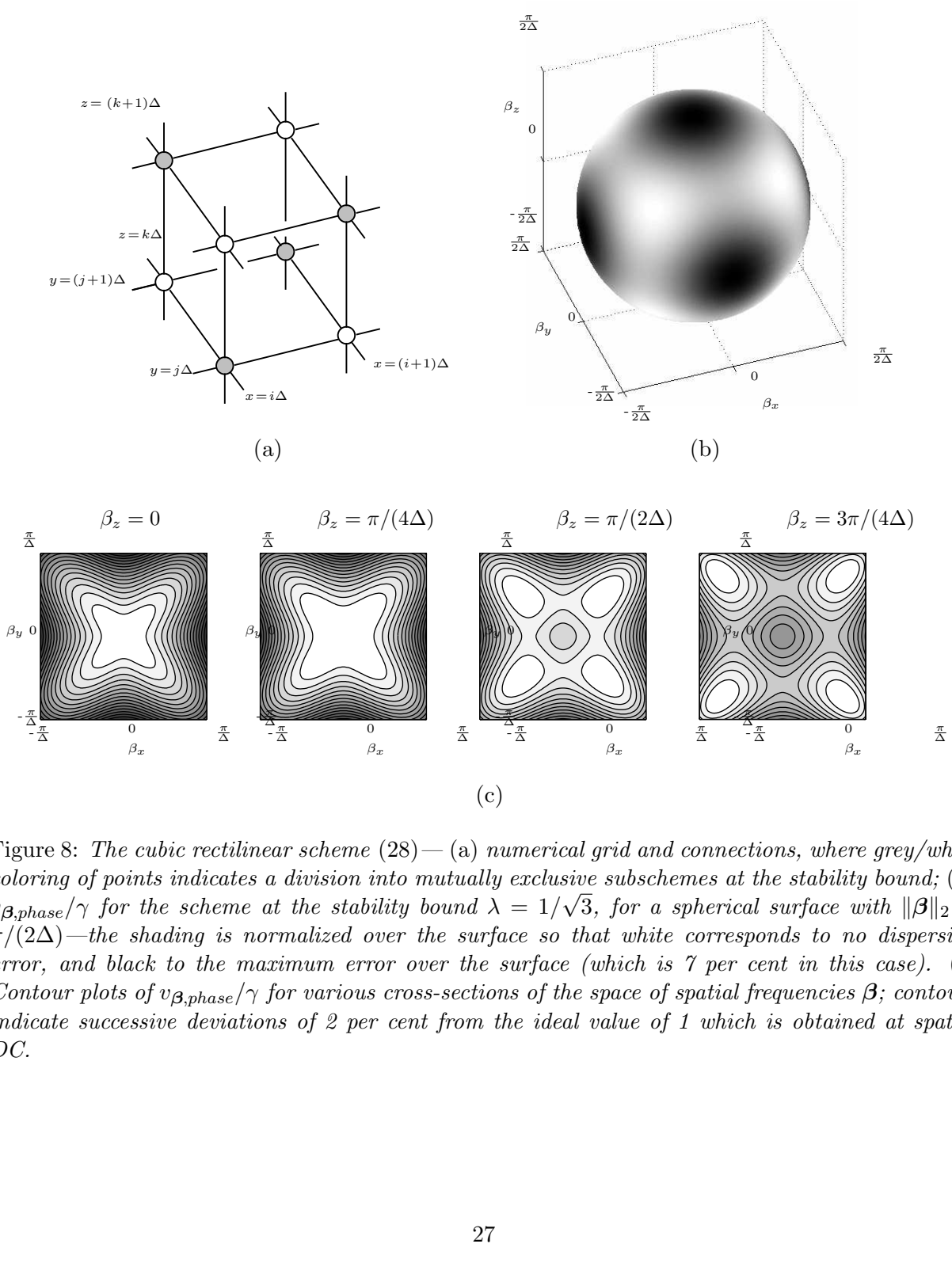

Figure 8: *The cubic rectilinear scheme* (28)— (a) *numerical grid and connections, where grey/white coloring of points indicates a division into mutually exclusive subschemes at the stability bound;* (b) $v_{\boldsymbol{\beta},phase}/\gamma$ *for the scheme at the stability bound* $\lambda = 1/\sqrt{3}$*, for a spherical surface with* $\|\boldsymbol{\beta}\|_2 = \pi/(2\Delta)$*—the shading is normalized over the surface so that white corresponds to no dispersion error, and black to the maximum error over the surface (which is 7 per cent in this case).* (c) *Contour plots of* $v_{\boldsymbol{\beta},phase}/\gamma$ *for various cross-sections of the space of spatial frequencies* $\boldsymbol{\beta}$*; contours indicate successive deviations of 2 per cent from the ideal value of 1 which is obtained at spatial DC.*

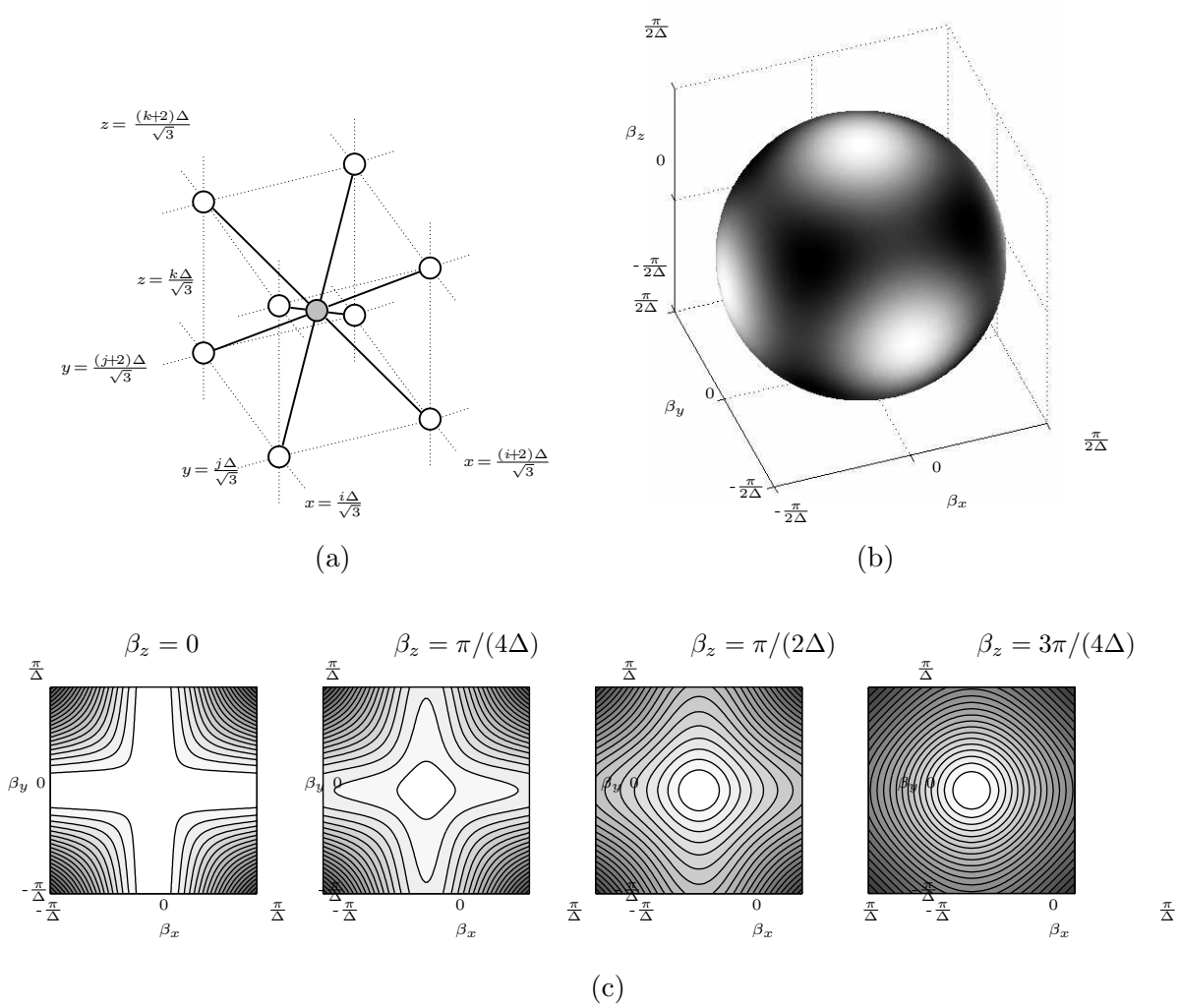

Figure 9: *The octahedral scheme* (29)— (a) *numerical grid and connections, where grey/white coloring of points indicates a division into mutually exclusive subschemes at the stability bound;* (b) $v_{\boldsymbol{\beta},phase}/\gamma$ *for the scheme at the stability bound* $\lambda = 1/\sqrt{3}$*, for a spherical surface with* $\|\boldsymbol{\beta}\|_2 = \pi/(2\Delta)$*—the shading is normalized over the surface so that white corresponds to no dispersion error, and black to the maximum error over the surface (which is 5 per cent in this case).* (c) *Contour plots of the* $v_{\boldsymbol{\beta},phase}/\gamma$ *for various cross-sections of the space of spatial frequencies* $\boldsymbol{\beta}$*; contours indicate successive deviations of 2 per cent from the ideal value of 1 which is obtained at spatial DC.*

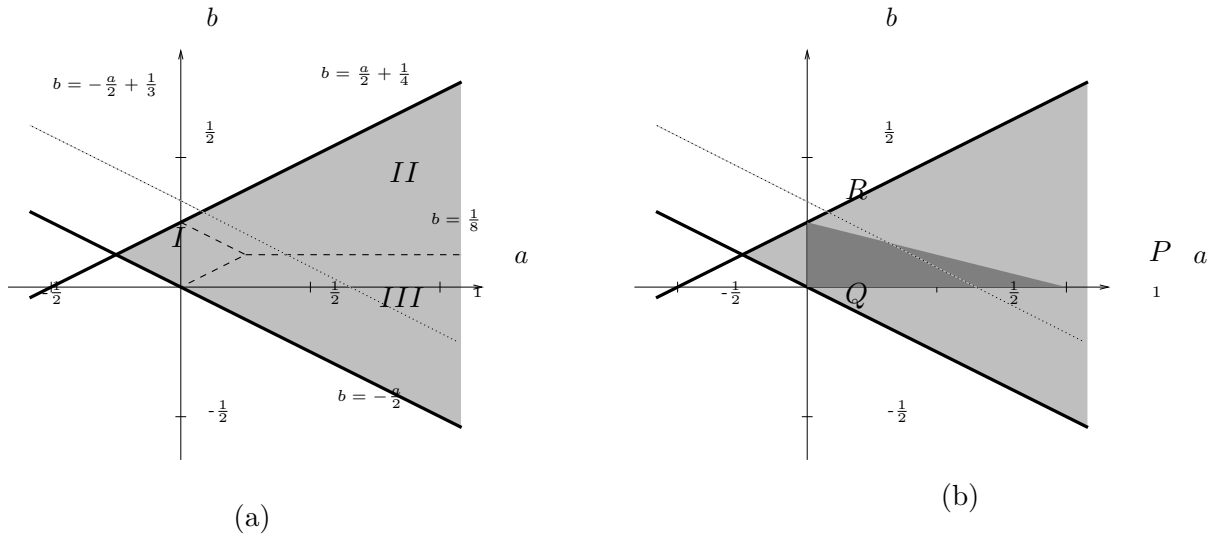

Figure 10: (a) *Stability region, in grey, for the interpolated rectilinear scheme, plotted in the* (a, b) *plane. This region can be divided into three sub-regions, labelled* I*,* II*, and* III *separated by dashed lines, over which different stability conditions on* λ *apply. In region* I*, we must have* $\lambda \leq 1$*, in region* II $\lambda \leq 1/\sqrt{2a + 4b}$*, and in region* III $\lambda \leq 1/\sqrt{2a - 4b + 1}$*. The dotted line indicates choices of* a *and* b *for which numerical dispersion is optimally direction-independent.* (b) *The subset of stable schemes for which a passive waveguide mesh implementation exists is shown in dark grey. Over this region, we require* $\lambda \leq 1/\sqrt{2a + 2b + 1}$*. This bound is more strict than the stability conditions mentioned above in the same region. We also remark that this interpolated scheme reduces to other simpler schemes under particular choices of* a *and* b*. At point* P*, we have the cubic rectilinear scheme (see §4.1), at point* Q *we have the octahedral scheme (see §4.2), and at point* R *we have what might be called a "dodecahedral" scheme. Notice in particular that none of these schemes is optimally direction-independent (i.e.,* P*,* Q *and* R *do not lie on the dotted line).*

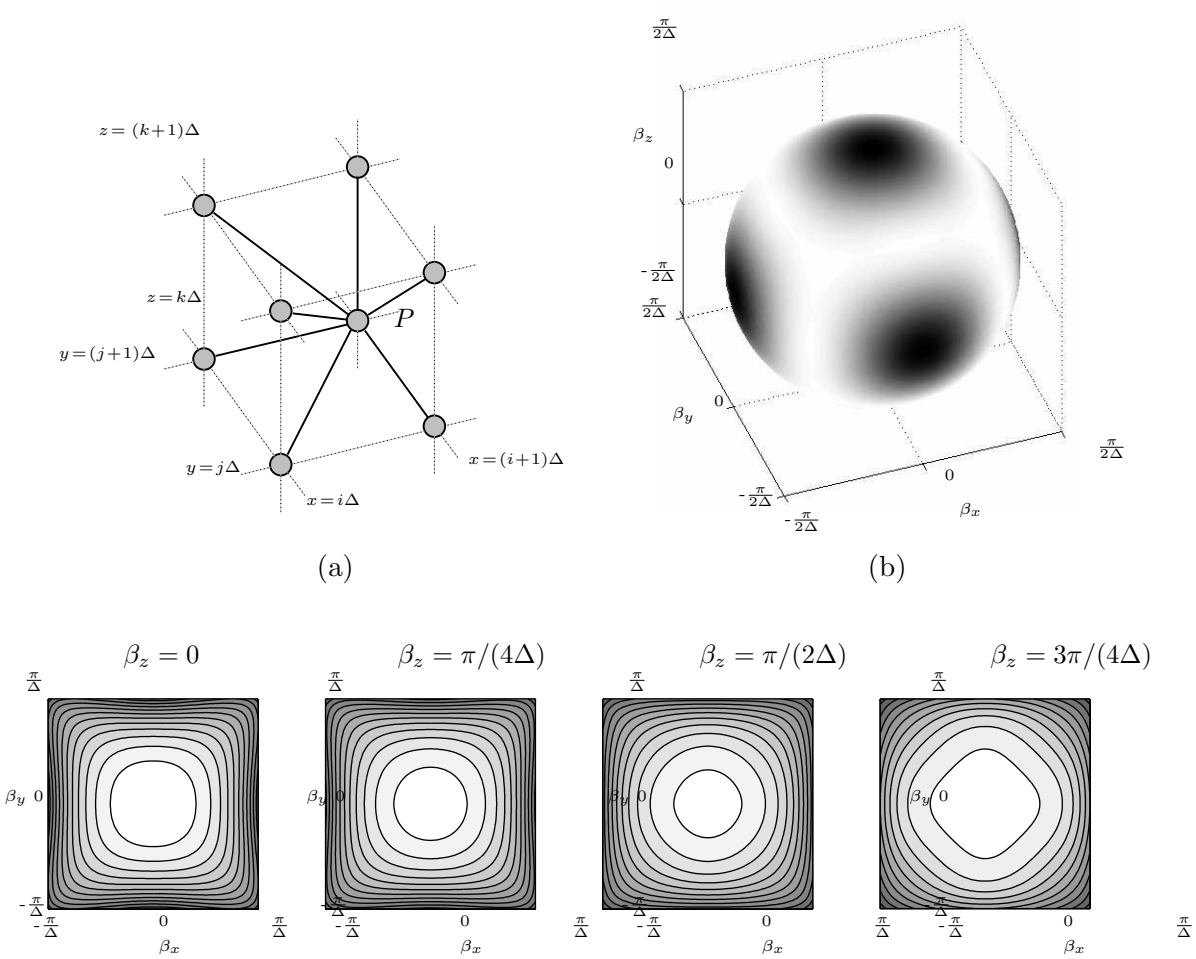

Figure 11: *The (3+1)D interpolated rectilinear scheme* (30)— (a) *numerical grid and connections, from a central grid point (labelled P) to its neighbors in one octant.* (b) $v_{\boldsymbol{\beta},phase}/\gamma$ *for the scheme with* $a = 0.42$ *and* $b = 0.1233$ *at the stability bound* $\lambda = 0.8617$*, for a spherical surface with* $\|\boldsymbol{\beta}\|_2 = \pi/(2\Delta)$*—the shading is normalized over the surface so that white and black refer to minimal and maximal dispersion error, respectively. Here, unlike for the cubic rectilinear and octahedral schemes, there are no dispersionless directions. The variation in the numerical phase velocity is, however, quite small, ranging from 96.81 to 97.32 per cent of the correct wave speed.* (c) *Contour plots of* $v_{\boldsymbol{\beta},phase}/\gamma$ *for various cross-sections of the space of spatial frequencies* $\boldsymbol{\beta}$*; contours indicate successive deviations of 2 per cent from the ideal value of 1 which is obtained at spatial DC.*

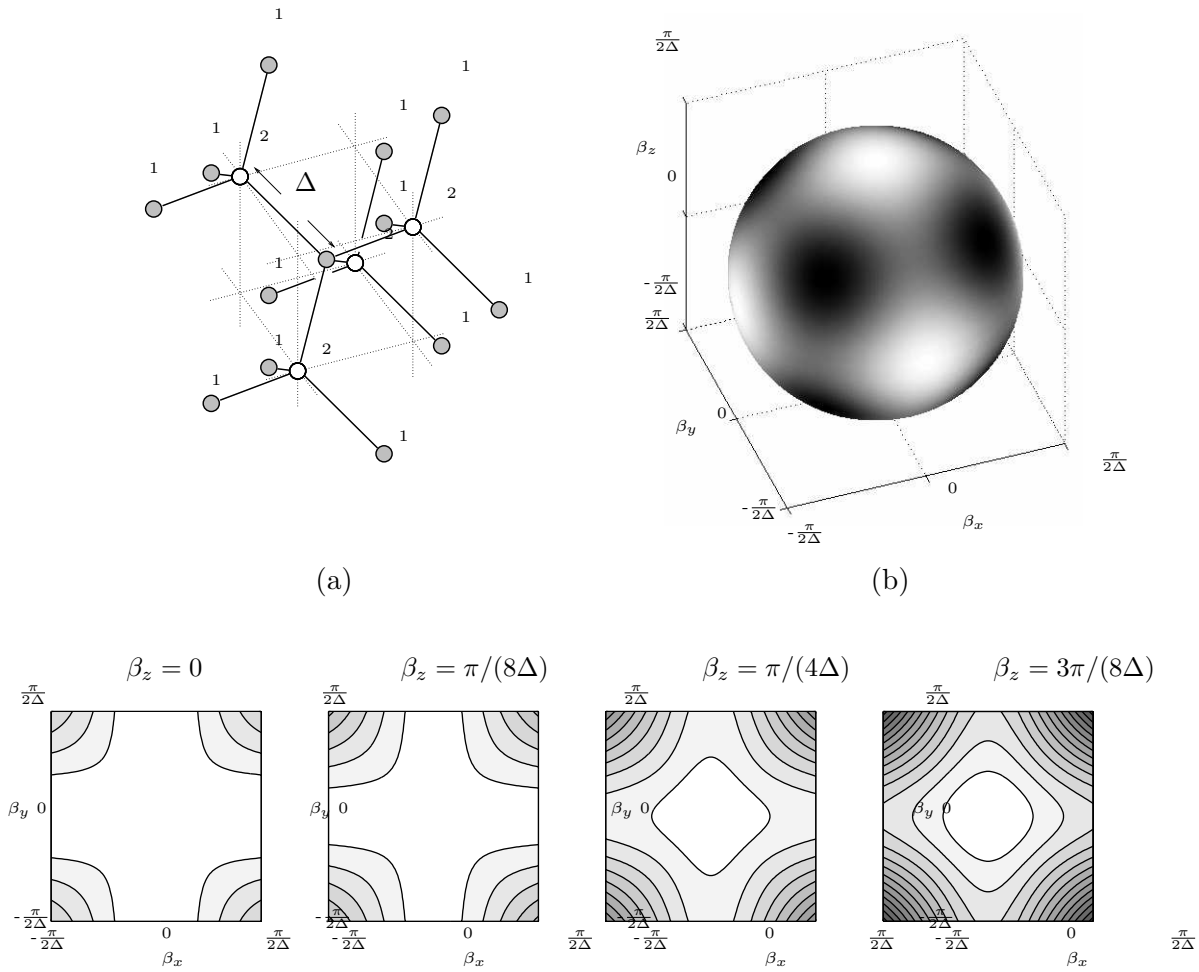

Figure 12: *The tetrahedral scheme* (32)— (a) *numerical grid and connections, where grey/white coloring of points indicates a division into mutually exclusive subschemes at the stability bound. The scheme can be indexed similarly to the octahedral scheme (see Figure 9). The two sub grids with mutually inverse orientations are labelled 1 and 2.* (b) $v_{\boldsymbol{\beta},phase}/\gamma$ *for the scheme at the stability bound* $\lambda = 1/\sqrt{3}$*, for a spherical surface with* $\|\boldsymbol{\beta}\|_2 = \pi/(2\Delta)$*—the shading is normalized over the surface so that white corresponds to no dispersion error, and black to the maximum error over the surface (which is 6 per cent in this case).* (c) *Contour plots of* $v_{\boldsymbol{\beta},phase}/\gamma$ *for various cross-sections of the space of spatial frequencies* $\boldsymbol{\beta}$*; contours indicate successive deviations of 2 per cent from the ideal value of 1 which is obtained at spatial DC. Here we have only plotted spatial frequencies to* $|\beta_x|$*,* $|\beta_y|$*, and* $|\beta_z|$ *all less than* $\pi/(2\Delta)$*.*

References

[1] R. Abraham, *Linear and Multilinear Algebra*, New York: W. A. Benjamin, Inc., 1966.

[2] S. Bilbao, *Wave and Scattering Methods for the Numerical Integration of Partial Differential Equations*, PhD thesis, Stanford University, June 2001, Available online at http://www-ccrma.stanford.edu/~bilbao/.

[3] L. Savioja, "Improving the three-dimensional digital waveguide mesh by interpolation," in *Proc. Nordic Acoustical Meeting (NAM'98)*, (Stockholm, Sweden), pp. 265–268, 7-9 Sept. 1998.

[4] L. Savioja and V. Välimäki, "Reducing the dispersion error in the digital waveguide mesh using interpolation and frequency-warping techniques," *IEEE Trans. Speech and Audio Proc.*, vol. 8, pp. 184–194, Mar. 2000.

[5] L. Savioja and V. Välimäki, "Interpolated 3-D digital waveguide mesh with frequaency warping," 7–11 May 2001, To appear.

[6] J. Stewart, *Calculus: Early Transcendentals*, Pacific Grove, California: Brooks/Cole, second ed., 1991.

[7] S. Stoffels, "Full mesh warping techniques," in *Proc. COST G-6 Conference on Digital Audio Effects*, (Verona, Italy), Dec. 7–9 2000.

[8] J. Strikwerda, *Finite Difference Schemes and Partial Differential Equations*, Pacific Grove, Calif.: Wadsworth and Brooks/Cole Advanced Books and Software, 1989.

[9] P. P. Vaidyanathan, *Multirate Systems and Filter Banks*, p. 288, Englewood Cliffs, New Jersey: Prentice-Hall, 1993.

[10] S. VanDuyne and J. S. III, "Physical modelling with the 2D digital waveguide mesh," in *Proc. Int. Computer Music Conf.*, (Tokyo, Japan), pp. 40–47, 1993.

[11] S. VanDuyne and J. Smith, "The 3D tetrahedral digital waveguide mesh with musical applications," in *Proc. Int. Computer Music Conf.*, (Hong Kong), pp. 9–16, 18–21 Aug. 1996.